Journal of Nuclear Medicine, published on March 19, 2021 as doi:10.2967/jnumed.120.248443

Rational Linker Design to Accelerate Excretion and Reduce Background Uptake of Peptidomimetic PSMA-Targeting Hybrid Molecules

Ann-Christin Eder[1,2,3,4*], Martin Schäfer[1], Jana Schmidt[1], Ulrike Bauder-Wüst[1], Mareike Roscher[1], Karin Leotta[4,5], Uwe Haberkorn[4,5], Klaus Kopka[1,6,#,†], Matthias Eder[2,3,†]

[†]These authors contributed equally to the study and share last authorship.

[1] Division of Radiopharmaceutical Chemistry, German Cancer Research Center (DKFZ), Heidelberg, Germany

[2] Department of Nuclear Medicine, University Medical Center Freiburg, University of Freiburg, Faculty of Medicine, Freiburg, Germany

[3] Division of Radiopharmaceutical Development, German Cancer Consortium (DKTK), partner site Freiburg, Freiburg, Germany and German Cancer Research Center, Heidelberg, Germany

[4] Department of Nuclear Medicine, Heidelberg University Hospital, Heidelberg, Germany

[5] Clinical Cooperation Unit Nuclear Medicine, German Cancer Research Center (DKFZ), Heidelberg, Germany

[6] German Cancer Consortium (DKTK), Heidelberg, Germany

[#] current address: Helmholtz-Zentrum Dresden-Rossendorf (HZDR), Institute of Radiopharmaceutical Cancer Research, Dresden, Germany

* First and corresponding author:
Dr. Ann-Christin Eder
Department of Nuclear Medicine, University Medical Center Freiburg and Division of Radiopharmaceutical Development, German Cancer Consortium, partner site Freiburg, and German Cancer Research Center, Heidelberg, Germany
Hugstetter Str. 55
79106 Freiburg
Tel: +49 761 270 63370
Fax: +49 761 270 39980
Email: ann-christin.eder@uniklinik-freiburg.de

Word count of the manuscript: 4996

Financial support: BMBF/VIP+ (VP00130)

Short running title:

Linker Design for PSMA Hybrid Molecules

ABSTRACT

The evolution of peptidomimetic hybrid molecules for preoperative imaging and guided surgery targeting the prostate-specific membrane antigen (PSMA) significantly progressed over the past years and some approaches are currently evaluated for further clinical translation. However, accumulation in non-malignant tissue such as kidney, bladder, spleen or liver might limit tumor-to-background contrast for precise lesion delineation particularly in a surgical setting. To overcome these limitations a rational linker design aims at the development of a second generation of PSMA-11 based hybrid molecules with enhanced pharmacokinetic profile and improved imaging contrasts. **Methods:** A selection of rational designed linkers was introduced to the PSMA-targeting hybrid molecule Glu-urea-Lys-HBED-CC-IRDye800CW resulting in a second generation peptidomimetic hybrid molecule library. The biological properties were investigated in cell-based assays. In a preclinical proof-of-concept study with the radionuclide ^{68}Ga, the impact of the modifications was evaluated by determination of specific tumor uptake, pharmacokinetics and fluorescence-imaging in tumor-bearing mice. **Results:** The modified hybrid molecules carrying various selected linkers revealed high PSMA-specific binding affinity and effective internalization. The highest tumor-to-background contrast of all modifications investigated was identified for the introduction of a histidine (H) and glutamic acid (E) containing linker ((HE)$_3$-linker) between PSMA-binding motif and chelator. In comparison to the parental core structure, uptake in non-malignant tissue was significantly reduced to a minimum exemplified by an 11-fold reduced spleen uptake from 38.12±14.62 %ID/g to 3.47±1.39 %ID/g (1 h p.i.). The specific tumor uptake of this compound (7.59±0.95 %ID/g, 1 h p.i.) was detected to be significantly higher as compared to the parental tracer PSMA-11. These findings confirmed by PET and fluorescence imaging are accompanied by an enhanced pharmacokinetic profile with accelerated background clearance at early time points post injection. **Conclusion:** The novel generation of PSMA-targeting hybrid molecules reveal fast elimination, reduced background organ enrichment and high PSMA-specific tumor uptake meeting the key demands

for potent tracers in Nuclear Medicine and fluorescence-guided surgery. The approach's efficacy of improving the pharmacokinetic profile highlights the strengths of rational linker design as a powerful tool in strategic hybrid molecule development.

Key words

PSMA; hybrid molecules; prostate cancer; guided-surgery; pharmacokinetic profile

INTRODUCTION

Surgical resection of tumor tissue represents one of the main curative treatment options in the clinical management of prostate cancer (*1*). The precise detection and comprehensive resection of malignancies is thereby of high significance for patient survival and therapy success. During resection several difficulties are limiting the therapeutic outcome. While malignant tissue can be precisely localized preoperatively using diagnostic radiopharmaceuticals, the translation to the operating theatre often remains challenging. This increases the risk of tumor tissue being missed out by the surgeon (*2,3*). Additionally, a close proximity of lesions to essential healthy structures such as urinary bladder or nerves impedes a wide dissection in the lower pelvis resulting in positive surgical margins (*4*). These difficulties cause an increased possibility of cancer recurrence and subsequent treatment failure (*5*). Consequently, for example template-based extended lymphadenectomies are performed to diminish the risk of left behind lesions (*6,7*). Besides malignant tissue, a considerable amount of healthy tissue is removed during this surgical strategy causing an increased morbidity. Hence, there is a strong medical need for advances in the field of intraoperative navigation to precisely delineate tumor tissue from surrounding healthy tissue.

To overcome these issues, novel approaches have been developed over the past years comprising the detection of malignant tissue supported by both a gamma probe and a fluorescent dye. A combination of these two modalities in so-called hybrid or dual-labeled approaches compensates for the respective disadvantages thereby merging the strength of both technologies. In a clinical scenario, these novel approaches provide preoperative imaging (e.g. PET/CT) for planning of the surgery combined with subsequent intraoperative navigation. First clinical proof-of-concept studies with the indocyanine green (ICG)-based hybrid sentinel lymph node tracer ICG-^{99m}Tc-NanoColloid demonstrated the feasibility of dual-modality approaches to improve surgical accuracy in different cancer types (*8-10*). As non-targeted approaches have

their limitations to precisely detect tumor tissue, recent advances focus on the design of targeted dual-modality probes.

For the specific targeting of prostate cancer, the prostate-specific membrane antigen (PSMA) has been identified as an excellent target structure. PSMA is a transmembrane carboxypeptidase, which is selectively overexpressed in the majority of prostate carcinomas, including local lesions, malignant lymph nodes and bone metastases (*11-14*). First PSMA-targeting dual-modality antibodies and small molecule peptidomimetic inhibitors have recently demonstrated their feasibility of hybrid detection in preclinical studies (*15-18*). Besides high and specific tumor uptake of targeted hybrid probes, a favorable pharmacokinetic profile with e.g. low accumulation in off-target tissue, fast clearance and a resulting high imaging contrast at early time points post injection is crucial for further clinical translation.

With the development of dual-modality low molecular weight PSMA-inhibitors based on the clinically established PET-tracer ^{68}Ga-PSMA-11, a versatile platform was designed tolerating the conjugation of a fluorescent dye combined with a radiolabel moiety (*18-20*). Our theranostic dual-modality platform is thus characterized by high and fast PSMA-specific tumor uptake along with rapid background clearance allowing preoperative imaging combined with intraoperative guidance (*18*). The advantageous effect of introducing spacer moieties comprising histidine (H) and glutamic acid (E) on the biodistribution profile of affibodies was originally reported by Hofstrom et al. (*21*). Further work from our group successfully established histidine/glutamic acid linker modifications to PSMA-11 leading to significantly enhanced tumor-to-background contrast and reduced uptake in dose limiting background organs (*22*). Due to the high clinical relevance, we introduced charged spacer moieties to our theranostic dual-modality platform leading to a second generation of hybrid probes with improved imaging contrasts. The insights investigated in this pharmacokinetic proof-of-concept study, demonstrate a valuable progression aiming at clinical translation for better management of prostate cancer patients.

METHODS

Chemical Synthesis, Radiolabeling, Determination of Lipophilicity and Serum Stability

The synthesis of the variants of Glu-urea-Lys-HBED-CC-IRDye800CW comprising a series of amino acid linker modifications was performed according to previously published protocols (*18,22-25*) (see Supplemental Data for details on the synthesis and chemical structures of the compounds). $^{68}Ga^{3+}$ (half-life 68 min; β^+ 89%; $E_{\beta+}$ max. 1.9 MeV) was obtained from a $^{68}Ge/^{68}Ga$ generator based on a pyrogallol resin support with details of compound characterization (radiolabeling, determination of lipophilicity, serum stability studies) provided in the Supplemental Data (*26*).

In Vitro Evaluation

PSMA-positive LNCaP cells (CRL-1740; ATCC) and PSMA-negative PC-3 cells (CRL-1435; ATCC) were cultured in RPMI medium supplemented with 10% fetal calf serum and 2 mmol/L L-glutamine (all from PAA). Cells were grown at 37°C in humidified air with 5% CO_2 and were harvested using trypsin-ethylenediaminetetraacetic acid (trypsin-EDTA; 0.25% trypsin, 0.02% EDTA, Invitrogen). Cell line authentication is regularly performed and the authentication of the LNCaP and PC-3 cell lines was confirmed on 03/06/2020. The competitive cell binding assay and internalization experiments were performed as described previously (*19,25*).

Biodistribution and Preclinical Proof-of-Concept

For the experimental tumor models 5×10^6 cells of LNCaP or PC-3 (in 50% Matrigel; Becton Dickinson) were subcutaneously inoculated into the flank of 7- to 8-week-old male BALB/c nu/nu mice (Charles River). For biodistribution studies, the ^{68}Ga-labeled compounds were injected into a tail vein (1-3 MBq; 60 pmol, n=3 and 30-50 MBq; 500 pmol, n=3). At 1 h and 2 h after injection, respectively, the animals were sacrificed. Organs of interest were dissected, blotted dry, and weighed. The radioactivity was measured using a gamma counter and calculated as % ID/g.

Optical imaging was performed with the Odyssey CLx system (LI-COR Biosciences, excitation wavelength 800 nm). In an additional preclinical proof-of-concept (n=1), mice were anesthetized (2% sevoflurane; Abbvie) and 0.5 nmol of the ^{68}Ga-labeled compound in 0.9% NaCl (pH 7) were injected into the tail vein. Preoperative PET imaging was performed with a PET scanner (Inveon PET; Siemens). For subsequent optical imaging to identify the tumor by fluorescence imaging, mice were sacrificed after PET imaging and dissected tissue analyzed using the Odyssey CLx system (see Supplemental Data for details on the imaging protocol, software, image reconstruction and procedure). All animal experiments were approved by the regional authorities *Regierungspräsidium Karlsruhe* and *Regierungspräsidium Freiburg* and complied with the current laws of the Federal Republic of Germany.

Statistical Aspects

Experiments were performed at least in triplicate except the proof-of-concept study (n=1). Quantitative data are expressed as mean ± SD. The n-values are given in the respective figure or table captions. If applicable, means were compared using Student´s *t* test (GraphPad Prism Version 8, GraphPad Software, Inc.). p-values < 0.05 were considered statistically significant.

RESULTS

Synthesis, Radiolabeling and Serum Stability

For this pharmacokinetic proof-of-concept study, Glu-urea-Lys-HBED-CC-IRDye800CW (tumor uptake 1 h p.i.: 13.66±3.73 %ID/g) was selected as exemplary model core structure of our theranostic dual-modality platform for two main reasons. First, this compound has been preclinically proven to perform comparably to or even outperformed successfully established molecules such as PSMA-11 (tumor uptake 1 h p.i.: 4.89±1.34 %ID/g) or PSMA-617 (tumor uptake 1 h p.i.: 8.47±4.09 %ID/g) (*18,22,27*). Second, the choice of the structure previously comprising the bulky clinically relevant NIR-dye IRDye800CW simplifies further clinical translation of the findings, since small molecules' biological properties are typically strongly influenced when conjugated to a fluorescent dye. In a first step, charged linker moieties identified favourable with respect to pharmacokinetic properties in previous studies were introduced combining solid phase and classical organic synthesis strategies (Supplemental Figs. 1 and 2) (*18,22*). As the most promising candidate in former studies, the $(HE)_3$-motif was additionally inserted between chelator and fluorescent moiety to investigate the influence of linker positioning within the molecule (Supplemental Fig. 2) (*23,28*). The dye was conjugated to the precursor molecules as IRDye800CW-NHS-ester in the last step. A detailed description of the synthetic strategies is provided in the Supplemental Information. The final products were obtained in >98% purity and their analytical data is summarized in the Supplemental Data (Supplemental Figs. 3 and 4; Supplemental Tables 1 and 2). Lipophilicity determined as log*D* at pH 7.4 in n-octanol/PBS was found to be in the same range compared to the respective Glu-urea-Lys-HBED-CC-IRDye800CW reference compound with a $\log D_{pH\ 7.4}$ value of - 2.21 ± 0.36 (Supplemental Table 1) (*18*). Radiolabeling with ^{68}Ga resulted in radiochemical yields >99% and the molar activities of the ^{68}Ga-labeled compounds were detected to be around 80-120 GBq/µmol (Supplemental Figs. 5-7). ^{68}Ga-Glu-urea-Lys-$(HE)_3$-HBED-CC-IRDye800CW was found to be stable in mouse and human serum up to 2 h.

PSMA-Specific Binding and Internalization Properties

High and specific affinity to PSMA in the nanomolar range was revealed for all tested compounds in competitive binding studies, which additionally was found to be not significantly complexation-dependent (Table 1; Supplemental Fig. 8). The introduction of $(HE)_1$- or trypotophane (W) containing $(WE)_1$-motifs between PSMA-binding motif and chelator or the $(HE)_3$-motif between chelator and fluorescent dye had no impact on binding properties as compared to the reference Glu-urea-Lys-HBED-CC-IRDye800CW (*18*). Interestingly, the $(HE)_3$-motif inserted between PSMA binding unit and chelator moiety significantly reduced the affinity to PSMA ($p=0.024$). Specific cell surface binding was detected for all tested dual-labeled probes (Table 1; Supplemental Fig. 9). Incorporating the $(WE)_1$- ($p=0.482$) or $(HE)_3$-motif ($p=0.053$) in close proximity to the PSMA-binding motif resulted in the most pronounced specifically internalized fractions not significantly differing from the reference (*18*). In contrast, changing the intramolecular $(HE)_3$-motif position by inserting the linker between chelator and dye ($p=0.021$) or introducing $(HE)_1$ as a linker structure next to the PSMA-binding motif ($p=0.021$) revealed significantly reduced internalization properties (Table 1).

Specific Enrichment in Xenograft Tumors with Enhanced Contrast to Background Tissue

The impact of the introduction of charged amino acid linker motifs to Glu-urea-Lys-HBED-CC-IRDye800CW on *in vivo* specific PSMA targeting and accompanying background organ enrichment was further evaluated in biodistribution studies. ^{68}Ga-Glu-urea-Lys-$(HE)_3$-HBED-CC-IRDye800CW revealed a significant higher, PSMA-specific tumor uptake in LNCaP xenograft tumors (7.59±0.95 %ID/g, $p<0.05$), compared to the incorporation of other motifs or intramolecular positioning of the $(HE)_3$-motif in closer proximity to the fluorescent dye at 1 h post injection (p.i.) (Fig. 1A, B; Supplemental Fig. 10; Supplemental Tables 3-5). Although in comparison to the core structure, tumor uptake was significantly reduced for ^{68}Ga-Glu-urea-Lys-$(HE)_3$-HBED-CC-IRDye800CW ($p=0.031$), it proved to be significantly higher when compared to

^{68}Ga-PSMA-11 (p=0.047) or ^{68}Ga-PSMA-I&F (p=0.045), and identical as compared to ^{68}Ga-PSMA-617 (p=0.735) (*17,22,27*). In addition, tracer uptake of ^{68}Ga-Glu-urea-Lys-$(HE)_3$-HBED-CC-IRDye800CW in non-malignant tissue was significantly reduced to a minimum with striking effects on e.g. spleen uptake, which could be reduced from 38.12±14.62 %ID/g to 3.47±1.39 %ID/g (Fig. 1A; Supplemental Table 3) (*18*). From the here presented series, the introduction of the $(HE)_3$-motif in close proximity to the PSMA-binding motif led to the highest tumor-to-background contrast. Noticeably, this compound even outperforms the core structure Glu-urea-Lys-HBED-CC-IRDye800CW with regard to tumor-to-background ratio (Supplemental Table 4). For all compounds the renal pathway was identified to be the most likely elimination mechanism.

Additionally, to finalize the analysis of the pharmacokinetic properties of the favoured compound ^{68}Ga-Glu-urea-Lys-$(HE)_3$-HBED-CC-IRDye800CW, biodistribution studies at 2 h p.i. were conducted (Fig. 1C, D; Supplemental Table 6). Specific tumor accumulation was significantly reduced after injection of 60 pmol (3.10±1.17 %ID/g) as compared to 1 h p.i. (7.59±0.95 %ID/g) (p=0.007). Contemporaneously, the compound was strongly excreted from background tissue resulting in remaining high tumor-to-background ratios up to 2 h p.i. (Supplemental Table 6). Administration of higher doses of ^{68}Ga-Glu-urea-Lys-$(HE)_3$-HBED-CC-IRDye800CW (500 pmol) mainly confirmed the findings and even results in higher tumor-to-background ratios for muscle 1 and 2 h p.i. (Fig. 1C, D; Supplemental Tables 7 and 8).

Small-Animal PET and Optical Imaging

Subsequent small-animal PET studies with ^{68}Ga-Glu-urea-Lys-$(HE)_3$-HBED-CC-IRDye800CW confirmed strong tumor uptake in the LNCaP xenograft model accompanied by rapid clearance from non-malignant tissue resulting in high imaging contrasts at early time points p.i. (Fig. 2 A-D). High PSMA-specificity was proven *in vivo* as no measurable uptake was observed in PSMA-negative PC-3 xenografts (Fig. 2 B). The corresponding time activity curves of the dynamic PET scan up to 60 min p.i. demonstrate rapid clearance from off-target tissue

(muscle, liver, heart), but continuous accumulation in bladder and kidney due to the renal pathway of excretion (Fig. 2 C).

In fluorescence imaging ^{68}Ga-labeled Glu-urea-Lys-$(HE)_3$-HBED-CC-IRDye800CW obtained high tumor uptake resulting in excellent tumor visualization and strong tumor-to-background contrasts (Fig. 3; Supplemental Figs. 11 and 12). Additionally, the renal excretion pathway and the significantly reduced spleen uptake detected based on radioactivity was fluorescently confirmed.

DISCUSSION

The development of dual-modality probes for preoperative imaging and intraoperative (radio- or fluorescence-) guidance specifically targeting PSMA represents a promising new strategy in the diagnosis and therapy of PCa. The improved detection of tumor tissue supported by both, a gamma signal and a fluorescent dye, might overcome current surgical limitations. Therefore, a novel class of dual-labeled low molecular weight PSMA inhibitors has recently been developed thereby successfully demonstrating their feasibility for clinical translation in preclinical proof-of-concept studies (*16-18*). In particular, a specific and sufficiently high tumor uptake combined with a fast pharmacokinetic profile resulting in high tumor-to-background contrasts at early time points post injection challenges low molecular weight hybrid tracer development. ^{68}Ga-Glu-urea-Lys-HBED-CC-IRDye800CW was the first PSMA-targeting low molecular weight hybrid probe characterized by a 3-fold increased tumor uptake compared to the parental molecule PSMA-11, while preserving a fast pharmacokinetic (PK) profile.

Nevertheless, like other peptidomimetic PSMA inhibitors this dual-modality approach results in excretion via the renal pathway and accumulation in non-malignant tissue (spleen). Probe enrichment close to the surgical field might hamper specific lesion detection in particular

close to the urinary system. Additionally, non-malignant accumulation might be of concern regarding toxicity issues during clinical translation of this approach.

To address this limitation, our study discovers rational hybrid molecule design as a promising tool to accelerate the PK profile accompanied by a preserved high tumor uptake. In particular, introduction of spacer moieties comprising histidine (H) and glutamic acid (E) proved favourable to modulate the biodistribution profile of affibodies and petidomimetic inhibitors thereby improving tumor-to-background contrast and potential uptake in dose limiting non-malignant tissue (*21-23*).

In the here presented study, rational linker design is applied on the peptidomimetic hybrid molecule Glu-urea-Lys-HBED-CC-IRDye800CW, the current lead of our theranostic dual-modality platform. Due to its favourable characteristics (high specific tumor uptake, fast PK properties) and successfully incorporated clinically relevant NIR-dye (simplified clinical translation of PK study findings), it was designated for a further proof-of-concept PK-modulation (*18*). The chemical motifs $(HE)_1$, $(HE)_3$ and $(WE)_1$ found to be beneficial in previous studies were selected for this approach (*21-23*).

Binding affinities of all second generation compounds resulting from the present study were in the low nanomolar range indicating negligible functional impact of the selected linker motifs. Nevertheless, inserting the (HE)-motif as a triplicate between PSMA binding motif and chelator slightly reduces PSMA affinity. While a single charged and/or lipophilic motif is tolerated in terms of affinity, motif repetitions might hamper the advantageous interactions of the chelator HBED-CC with the arene binding side of the PSMA binding pocket (*29*). Specific internalization of all modifications was observed to be highest for the tryptophan-containing motif located close to the PSMA-binding motif, hypothetically exploiting supportive lipophilic interactions in the PSMA funnel (*30*).

However, the determined advantageous *in vitro* properties of $(HE)_1$- and $(WE)_1$-motif introduction did not result in an increased tumor uptake. While $(HE)_1$ and $(WE)_1$ located between the PSMA binding unit and the radiometal chelator significantly enhanced tumor uptake in previous findings (*22*), the effect could not be demonstrated in this study. Strikingly, including the $(HE)_3$-motif at the same intramolecular location resulted in a strongly improved background organ enrichment profile of the hybrid molecule at early time points post injection (1 h p.i.). In particular, spleen uptake was reduced by a factor of 11 when compared to the parental structure ^{68}Ga-Glu-urea-Lys-HBED-CC-IRDye800CW matching findings of earlier studies (*22*). In addition, this modification revealed the highest tumor-to-background ratios to relevant non-malignant tissue of all tested compounds including the parental structure. The resulting tumor uptake was significantly higher as compared to all the other modified variants of this study, including PSMA-11 and PSMA-I&F, however not exceeding the core structure Glu-urea-Lys-HBED-CC-IRDye800CW and PSMA-617 (*17,19,27*). Accordingly, it can be concluded that the novel compound features superior characteristics in terms of tumor uptake and tumor-to-background contrast warranting further investigation.

Thus, the exact intramolecular position of $(HE)_3$ was found to be highly crucial, as an introduction on a different location in the molecule results in significantly reduced or even negative effects on background organ enrichment and tumor uptake. The introduction of $(HE)_3$ in close proximity to the PSMA binding motif was found to noticeably influence for instance the spleen uptake, which is in line with previous studies (*22*).

The improved background organ enrichment profile of the novel hybrid molecule ^{68}Ga-Glu-urea-Lys-$(HE)_3$-HBED-CC-IRDye800CW was accompanied by a significantly accelerated excretion via the renal pathway by means of reduced kidney enrichment as compared to the parental structure ^{68}Ga-Glu-urea-Lys-HBED-CC-IRDye800CW leading to high tumor-to-background-contrast as early as 1 h p.i., which proved persistent up to 2 h p.i. (*18*). Surprisingly,

at 1 h p.i., the PK-improved compound showed an about 60 minutes earlier manifestation of the high tumor-to-background contrast as compared to the parental compound. This is caused by a dramatically minimized enrichment in non-malignant tissue leading to 2.0-fold higher tumor-to-blood and 1.6-fold higher tumor-to-muscle ratio at early time points after injection of 60 pmol. Consequently, an increased contrast in the surgical field can be expected from these data encouraging further clinical translation. Since other dyes are also being discussed in terms of e.g. stability, brightness or tissue penetration, further studies might identify the ideal combination finally representing the lead second generation PSMA-targeting hybrid probe.

CONCLUSION

This study discovers rational linker design as a powerful tool in hybrid molecule development leading to a novel generation of PSMA-targeting peptidomimetic hybrid molecules with significantly improved PK profile. With fast elimination and subsequent reduced enrichment in non-malignant tissue, this approach addresses the highly disruptive factor of background accumulation during surgical resection, while preserving a high PSMA-specific tumor uptake. The PK modification strategy uncovered in this study, offers extensive utility in the future discovery and development of targeted peptidomimetic hybrid agents.

DISCLOSURE

MS, UBW, UH, ME, KK, ACE hold patent rights on dual-labeled PSMA inhibitors. All other authors declare no competing interests.

ACKNOWLEDGEMENTS

We gratefully acknowledge support by the VIP+ grant VP00130, Federal Ministry of Education & Research (BMBF), Germany.

KEY POINTS

Question

Is the tool of rational linker design suitable for peptidomimetic hybrid molecule development to improve the pharmacokinetic profile and elimination rate?

Pertinent Findings

This preclinical proof-of-concept study discovers rational linker design as a valuable tool to selectively affect the pharmacokinetic profile and elimination rate of PSMA-targeted peptidomimetic hybrid molecules. By introducing a designated sequence of amino acids, enrichment in non-malignant tissue was significantly reduced to a minimum thereby also enhancing the elimination profile, while a high specific tumor uptake was preserved.

Implications for Patient Care

Background organ accumulation of novel hybrid molecules in e.g. the surgical field represents one of the main challenges in hybrid molecule development. The study findings introduce a tool to overcome these limitations and further advance discovery in novel image-guided surgery approaches for clinical translation.

REFERENCES

1. Cornford P, van den Bergh RCN, Briers E, et al. EAU-EANM-ESTRO-ESUR-SIOG Guidelines on prostate cancer. Part II-2020 Update: Treatment of relapsing and metastatic prostate cancer. *Eur Urol.* 2020.

2. Weckermann D, Dorn R, Trefz M, Wagner T, Wawroschek F, Harzmann R. Sentinel lymph node dissection for prostate cancer: experience with more than 1,000 patients. *J Urol.* 2007;177:916-920.

3. Mattei A, Fuechsel FG, Bhatta Dhar N, et al. The template of the primary lymphatic landing sites of the prostate should be revisited: results of a multimodality mapping study. *Eur Urol.* 2008;53:118-125.

4. Yossepowitch O, Briganti A, Eastham JA, et al. Positive surgical margins after radical prostatectomy: a systematic review and contemporary update. *Eur Urol.* 2014;65:303-313.

5. Stephenson AJ, Eggener SE, Hernandez AV, et al. Do margins matter? The influence of positive surgical margins on prostate cancer-specific mortality. *Eur Urol.* 2014;65:675-680.

6. Munbauhal G, Seisen T, Gomez FD, et al. Current perspectives of sentinel lymph node dissection at the time of radical surgery for prostate cancer. *Cancer Treat Rev.* 2016;50:228-239.

7. Kiss B, Thoeny HC, Studer UE. Current status of lymph node imaging in bladder and prostate cancer. *Urology.* 2016;96:1-7.

8. van der Poel HG, Buckle T, Brouwer OR, Valdes Olmos RA, van Leeuwen FW. Intraoperative laparoscopic fluorescence guidance to the sentinel lymph node in prostate cancer patients: clinical proof of concept of an integrated functional imaging approach using a multimodal tracer. *Eur Urol.* 2011;60:826-833.

9. Brouwer OR, Buckle T, Vermeeren L, et al. Comparing the hybrid fluorescent-radioactive tracer indocyanine green-99mTc-nanocolloid with 99mTc-nanocolloid for sentinel node identification: a validation study using lymphoscintigraphy and SPECT/CT. *J Nucl Med.* 2012;53:1034-1040.

10. KleinJan GH, van den Berg NS, de Jong J, et al. Multimodal hybrid imaging agents for sentinel node mapping as a means to (re)connect nuclear medicine to advances made in robot-assisted surgery. *Eur J Nucl Med Mol Imaging.* 2016;43:1278-1287.

11. Silver DA, Pellicer I, Fair WR, Heston WD, Cordon-Cardo C. Prostate-specific membrane antigen expression in normal and malignant human tissues. *Clin Cancer Res.* 1997;3:81-85.

12. Wright GL, Jr., Haley C, Beckett ML, Schellhammer PF. Expression of prostate-specific membrane antigen in normal, benign, and malignant prostate tissues. *Urol Oncol.* 1995;1:18-28.

13. Sweat SD, Pacelli A, Murphy GP, Bostwick DG. Prostate-specific membrane antigen expression is greatest in prostate adenocarcinoma and lymph node metastases. *Urology.* 1998;52:637-640.

14. Minner S, Wittmer C, Graefen M, et al. High level PSMA expression is associated with early psa recurrence in surgically treated prostate cancer. *Prostate.* 2011;71:281-288.

15. Lutje S, Rijpkema M, Franssen GM, et al. Dual-modality image-guided surgery of prostate cancer with a radiolabeled fluorescent anti-PSMA monoclonal antibody. *J Nucl Med.* 2014;55:995-1001.

16. Banerjee SR, Pullambhatla M, Byun Y, et al. Sequential SPECT and optical imaging of experimental models of prostate cancer with a dual modality inhibitor of the prostate-specific membrane antigen. *Angew Chem Int Ed Engl.* 2011;50:9167-9170.

17. Schottelius M, Wurzer A, Wissmiller K, et al. Synthesis and preclinical characterization of the PSMA-targeted hybrid tracer PSMA-I&F for nuclear and fluorescence imaging of prostate cancer. *J Nucl Med.* 2019;60:71-78.

18. Baranski AC, Schafer M, Bauder-Wust U, et al. PSMA-11-derived dual-labeled PSMA inhibitors for preoperative PET imaging and precise fluorescence-guided surgery of prostate cancer. *J Nucl Med.* 2018;59:639-645.

19. Eder M, Schafer M, Bauder-Wust U, et al. 68Ga-complex lipophilicity and the targeting property of a urea-based PSMA inhibitor for PET imaging. *Bioconjug Chem.* 2012;23:688-697.

20. Hope TA, Aggarwal R, Chee B, et al. Impact of (68)Ga-PSMA-11 PET on management in patients with biochemically recurrent prostate cancer. *J Nucl Med.* 2017;58:1956-1961.

21. Hofstrom C, Orlova A, Altai M, Wangsell F, Graslund T, Tolmachev V. Use of a HEHEHE purification tag instead of a hexahistidine tag improves biodistribution of affibody molecules site-specifically labeled with (99m)Tc, (111)In, and (125)I. *J Med Chem.* 2011;54:3817-3826.

22. Baranski AC, Schafer M, Bauder-Wust U, et al. Improving the imaging contrast of (68)Ga-PSMA-11 by targeted linker design: charged spacer moieties enhance the pharmacokinetic properties. *Bioconjug Chem.* 2017;28:2485-2492.

23. Eder M, Lohr T, Bauder-Wust U, et al. Pharmacokinetic properties of peptidic radiopharmaceuticals: reduced uptake of (EH)3-conjugates in important organs. *J Nucl Med.* 2013;54:1-4.

24. Eder M, Wangler B, Knackmuss S, et al. Tetrafluorophenolate of HBED-CC: a versatile conjugation agent for 68Ga-labeled small recombinant antibodies. *Eur J Nucl Med Mol Imaging.* 2008;35:1878-1886.

25. Schafer M, Bauder-Wust U, Leotta K, et al. A dimerized urea-based inhibitor of the prostate-specific membrane antigen for 68Ga-PET imaging of prostate cancer. *EJNMMI Res.* 2012;2:23.

26. Schuhmacher J, Maier-Borst W. A new Ge-68/Ga-68 radioisotope generator system for production of Ga-68 in dilute HCl. *Int J Appl Radiat Isot.* 1981;32:31–36.

27. Benesova M, Schafer M, Bauder-Wust U, et al. Preclinical evaluation of a tailor-made DOTA-conjugated PSMA inhibitor with optimized linker moiety for imaging and endoradiotherapy of prostate cancer. *J Nucl Med.* 2015;56:914-920.

28. Liolios C, Schafer M, Haberkorn U, Eder M, Kopka K. Novel bispecific PSMA/GRPr targeting radioligands with optimized pharmacokinetics for improved PET imaging of prostate cancer. *Bioconjug Chem.* 2016;27:737-751.

29. Zhang AX, Murelli RP, Barinka C, et al. A remote arene-binding site on prostate specific membrane antigen revealed by antibody-recruiting small molecules. *J Am Chem Soc.* 2010;132:12711-12716.

30. Mesters JR, Barinka C, Li W, et al. Structure of glutamate carboxypeptidase II, a drug target in neuronal damage and prostate cancer. *EMBO J.* 2006;25:1375-1384.

FIGURES

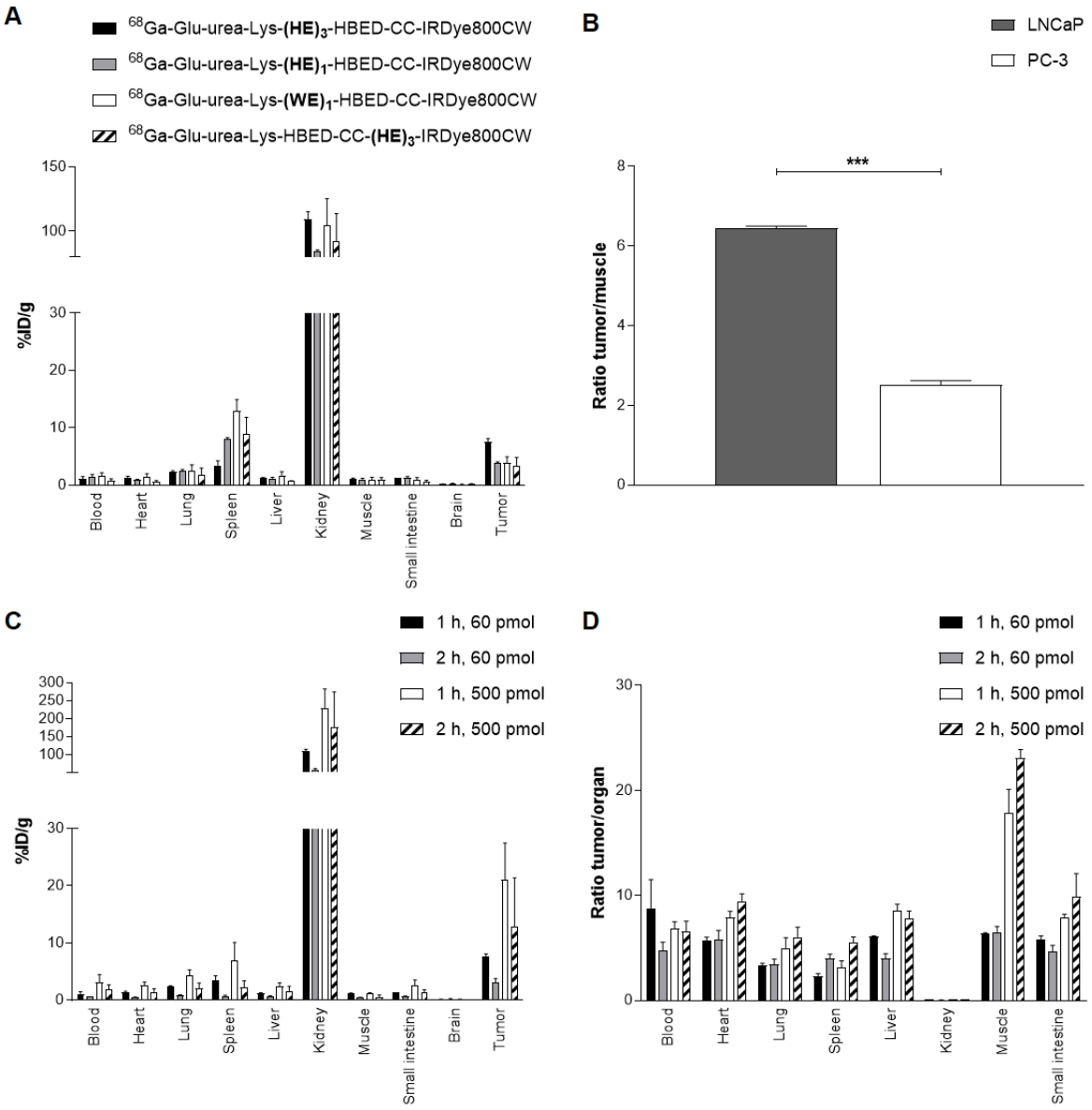

Figure 1. Organ distribution of ^{68}Ga-labeled compounds. (A) Organ distribution of 60 pmol ^{68}Ga-labeled compounds at 1 h p.i. (LNCaP) with statistics shown in Supplemental Fig. 10, (B) LNCaP- in comparison to PC-3-tumor-to-muscle ratio of 60 pmol ^{68}Ga-labeled Glu-urea-Lys-(HE)$_3$-HBED-CC-IRDye800CW 1 h p.i. (***p<0.001), (C) organ distribution and (D) tumor-to-organ ratios of 60 pmol and 500 pmol ^{68}Ga-labeled Glu-urea-Lys-(HE)$_3$-HBED-CC-IRDye800CW at 1 and 2 h p.i. in LNCaP-tumor bearing BALB/c nu/nu mice. Data are expressed as mean % ID/g tissue ± SD (n=3).

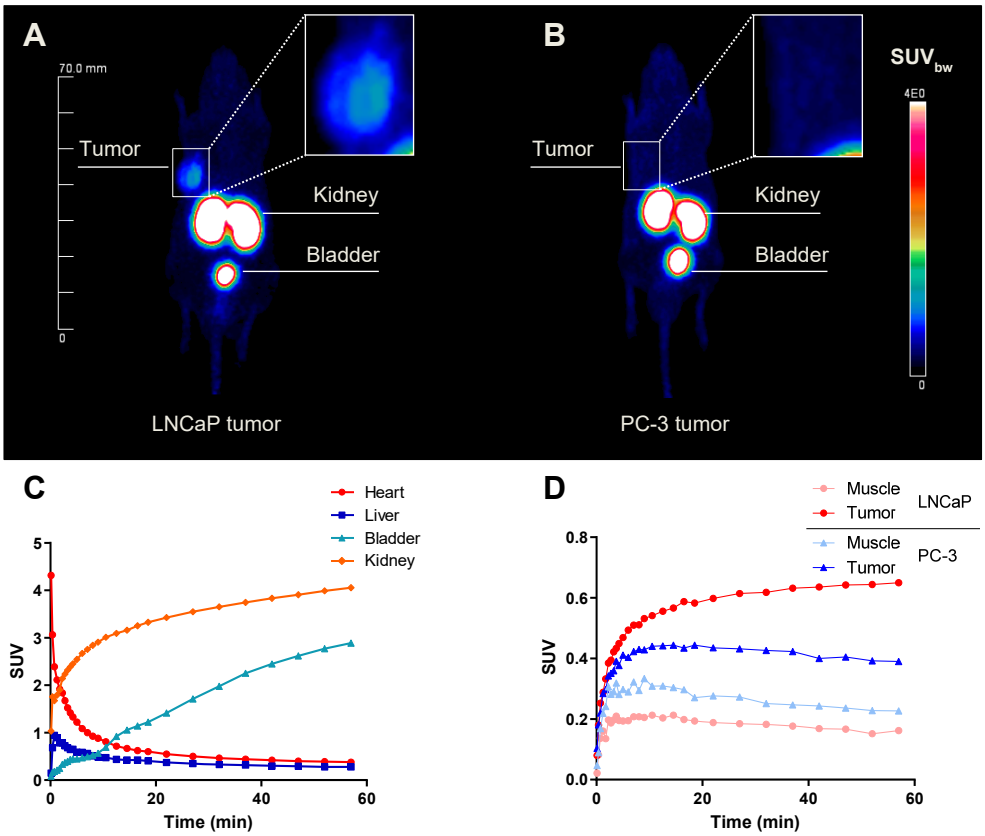

447 **Figure 2. Small-animal PET imaging study.** Whole-body maximum intensity projections with tumor magnifications of
448 0.5 nmol ^{68}Ga-labeled Glu-urea-Lys-(HE)$_3$-HBED-CC-IRDye800CW (~50 MBq) in LNCaP- (A) and PC-3- (B) tumor-
449 bearing BALB/c nu/nu mice (right flank) 120 min p.i. obtained from small animal PET imaging (n=1). Corresponding
450 time activity curves are shown in (C) for background organs and (D) for tumor and muscle. SUV=standardized uptake
451 value.

452

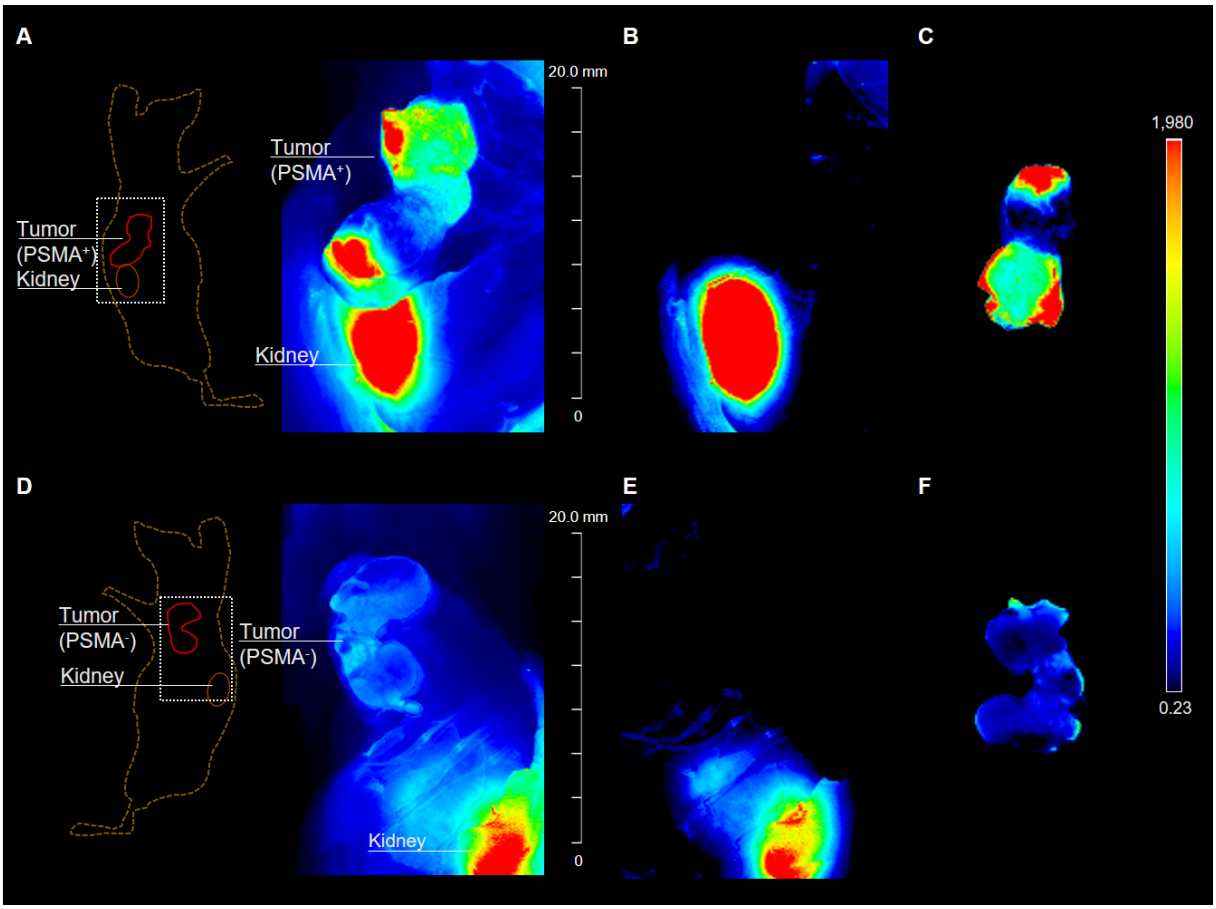

Figure 3. Optical imaging of tumor dissection. Optical imaging was performed after injection of 0.5 nmol ^{68}Ga-labeled Glu-urea-Lys-(HE)$_3$-HBED-CC-IRDye800CW in LNCaP (A)-(C) and PC-3 (D)-(F) tumor-bearing BALB/c nu/nu mice (n=1). Mice were sacrificed 2 h p.i. after PET imaging and fluorescence detected with the Odyssey CLx system (excitation wavelength 800 nm). Fluorescence intensity is presented in heat map colouring. Skin was removed covering the subcutaneous xenograft tumors and imaging was performed to locate the tumor (A)/(D). Tumor tissue was resected and another scan performed to ensure complete tumor tissue removal (B)/(E). Fluorescence signal of the resected tumors is presented in (C)/(F). Tissue lying on the surface of the imaging system during fluorescence detection explains small artefacts in fluorescence images.

TABLES

Table 1. Cell binding and internalization data of the compounds*. Affinity to PSMA and internalization properties of the compounds were determined *in vitro* using PSMA$^+$-cells (LNCaP). For all compounds PSMA-specific internalization and a not significantly complexation-dependent high binding affinity to PSMA in the low nanomolar range were detected.

Compound	Specifically cell surface bound [%AR/10^5 cells]†	Specifically internalized [%AR/10^5 cells]†	IC_{50} [nM]‡ free ligands	IC_{50} [nM]‡ $^{69/71}$Ga-labeled compounds
Glu-urea-Lys-**(HE)$_1$**-HBED-CC-IRDye800CW	3.00 ± 1.42	3.27 ± 1.83	28.41 ± 14.39	35.57 ± 22.83
Glu-urea-Lys-**(WE)$_1$**-HBED-CC-IRDye800CW	6.47 ± 3.69	13.77 ± 8.50	43.70 ± 14.12	56.80 ± 17.10
Glu-urea-Lys-**(HE)$_3$**-HBED-CC-IRDye800CW	8.30 ± 3.93	6.45 ± 3.36	51.39 ± 11.84	69.98 ± 22.88
Glu-urea-Lys-HBED-CC-**(HE)$_3$**-IRDye800CW	6.26 ± 1.49	3.70 ± 0.51	41.74 ± 18.26	52.21 ± 7.33

***** Data are expressed as mean ± SD (n=3), † ^{68}Ga-labeled compounds. Specific cell uptake was determined by blockage using 500 µM 2-PMPA. Values are expressed as % of applied radioactivity (AR) bound to 10^5 cells. ‡ radioligand: ^{68}Ga-PSMA-10 (K_d: 3.8 ± 1.8 nM (*25*), $c_{radioligand}$: 0.75 nM)

GRAPHICAL ABSTRACT

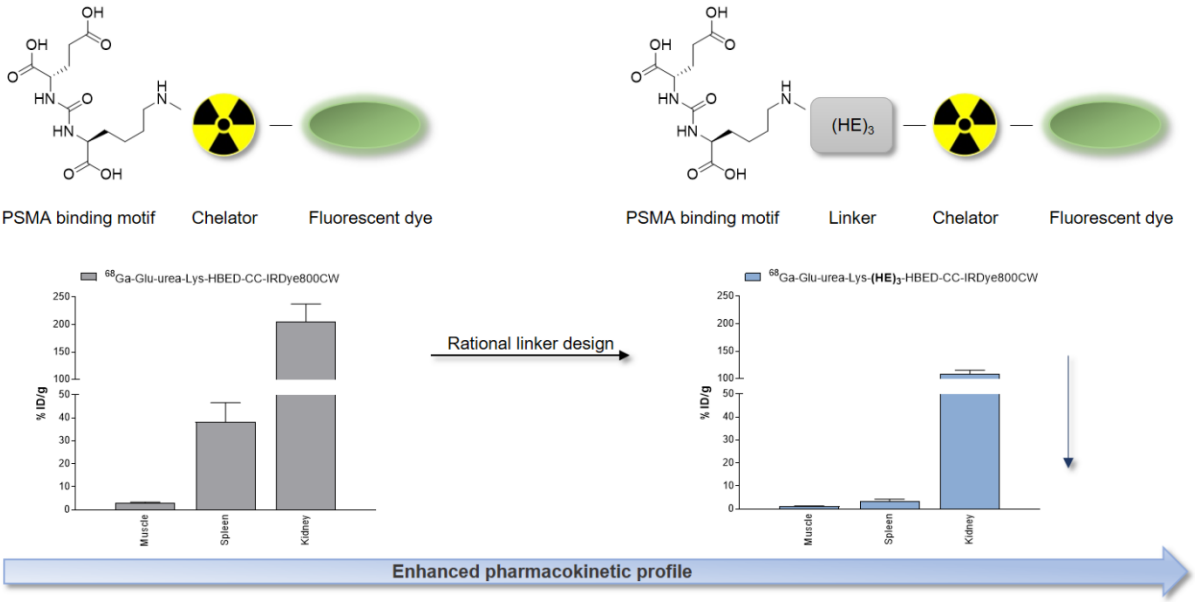

Supplementary Information

Compound Synthesis and Characterization

All commercially available chemicals were of analytical grade and used without further purification. Preparative HPLC was performed with the system LaPrep P110 (VWR) supplied with a variable UV detector (P314, VWR) and a NUCLEODUR® Sphinx RP column (VP250/21, 5 µm 250 x 21 mm; Macherey-Nagel). The system Agilent 1100 series (Agilent Technologies) was used for semipreparative and analytical HPLC runs thereby analyzing the compounds with reversed-phase high performance liquid chromatography (RP-HPLC; Chromolith RP-18e, 100×10mm/Chromolith RP-18e, 100×4.6 mm; Merck). For semipreparative HPLC runs a linear gradient (0.1% aqueous TFA (A) to 100% B (0.1% TFA in CH_3CN)) in 10 min at 5 mL/min and for analytical HPLC runs a linear gradient (0.1% aqueous TFA (A) to 100% B (0.1% TFA in CH_3CN)) in 10 min at 2 mL/min were selected. UV absorbance was measured at 214 and 254 nm, respectively. For all final products, the chemical purity was greater than 98%, as determined by HPLC. Analytical reversed-phase HPLC of the ^{68}Ga-labeled compound Glu-urea-Lys-$(HE)_3$-HBED-CC-IRDye800CW was performed using a EC 250/4.6 NUCLEOSIL 120-5 C 18 column (Machery-Nagel) with a linear gradient 85% 0.1% aqueous TFA (A) to 60% B (0.1% TFA in CH3CN)) in 13 min at 1.5 mL/min or a Chromolith RP-18e 100x4.6 mm column with a linear gradient (0.1% aqueous TFA (A) to 100% B (0.1 % TFA in CH3CN)) in 5 min at 4 mL/min. For mass spectrometry a MALDI-MS (Daltonics Microflex, Bruker Daltonics) and 2,5-dihydroxybenzoic acid as a matrix were used.

Synthesis of Glu-urea-Lys-$(HE)_1$-HBED-CC-IRDye800CW, Glu-urea-Lys-$(HE)_3$-HBED-CC-IRDye800CW and Glu-urea-Lys-$(WE)_1$-HBED-CC-IRDye800CW

Synthesis of Glu-urea-Lys-$(HE)_1$-$CO(CH_2)_4$-N_3, Glu-urea-Lys-$(WE)_1$-$CO(CH_2)_4$-N_3 and Glu-urea-Lys-$(HE)_3$-$CO(CH_2)_4$-N_3

The pharmacophore Glu-urea-Lys was synthesized as described previously (*1*). Briefly, the isocyanate of the glutamyl moiety was formed using triphosgene in a first step. Resin-immobilized (2-chloro-tritylresin) and ε-allyloxycarbonyl protected lysin was added, the reaction stirred for 16 h at room temperature and the resin was finally filtered off. By reacting twice with $Pd(PPh_3)_4$ (0.3 eq.) and morpholine (15 eq.) in dichloromethane under ambient conditions (1 h, RT, protected from light) the allyloxy-protecting group was cleaved. To build up the different linkers the resin was split and further continued with standard Fmoc solid phase protocols. Depending on the linker sequence the coupling of the amino acids Fmoc-L-His(Trt)-OH, Fmoc-L-Glu(O*t*-Bu)-OH or Fmoc-L-Trp(Boc)-OH, 4 eq. respectively, and as a final building block 5-azidopentanoic acid (4 eq.) was performed using HBTU (4 eq.) and DIPEA (4 eq.) in DMF.

Cleavage of the products from the resin was performed for 3 hours at RT using TFA/TIPS/H_2O (95/2.5/2.5, v/v/v) resulting in the azido-functionalized intermediates, which were purified using RP-HPLC and identified via mass spectrometry.

Synthesis of Glu-urea-Lys-$(HE)_1$-HBED-CC-PEG_2, Glu-urea-Lys-$(WE)_1$-HBED-CC-PEG_2 and Glu-urea-Lys-$(HE)_3$-HBED-CC-PEG_2

As described previously, HBED-CC$(TFP)_2$ was synthesized under Fe^{3+} protection and via the formation of $[Fe(HBED\text{-}CC)]^-$ (*2*). After isolating the bis-TFP ester with preparative HPLC, [Fe (HBED-CC)]TFP_2 and 0.95 eq. of propargylamine were dissolved in DMF in the presence of DIPEA (Supplemental Figure 1). An excess of 2,2′-(ethylenedioxy)bis(ethylamine) (100 µL) was added after 4 h at RT and the resulting mixture gently stirred for 16 h at RT. The alkenyl-functionalized chelator was finally purified using preparative HPLC. Afterwards, PEG_2-[Fe(HBED-CC-propargylamine)] (1 eq.) was reacted with the azido-functionalized intermediates

of the previous step (1 eq., respectively) via CuAAC, $CuSO_4$ (1 eq.), Na-ascorbate (1 eq.), in 3 mL THF/H_2O (1:1, v/v) for 16 h at RT. The Fe-protected products were purified by preparative HPLC and identified with mass spectrometry.

Conjugation of IRDye800CW

IRDye800CW-NHS ester (1 eq.) was conjugated to Glu-urea-Lys-$(HE)_1$-[Fe(HBED-CC-PEG_2-NH_2)], Glu-urea-Lys-$(WE)_1$-[Fe(HBED-CC-PEG_2-NH_2)] and Glu-urea-Lys-$(HE)_3$-[Fe(HBED-CC-PEG_2-NH_2)], respectively, in PBS-buffer (pH 8.5) for 24 h at RT. The Fe-protected products were isolated via semipreparative HPLC and identified with mass spectrometry. Complexed Fe^{3+} was removed as described previously (*2*). Briefly, the Fe-containing products were trapped on a C18 cartridge. Subsequently, the cartridge was flushed with 10 mL 1 M HCl and washed with 5 mL H_2O. The final products were eluted with 2 mL H_2O/CH_3CN (3:1) and evaporated to dryness.

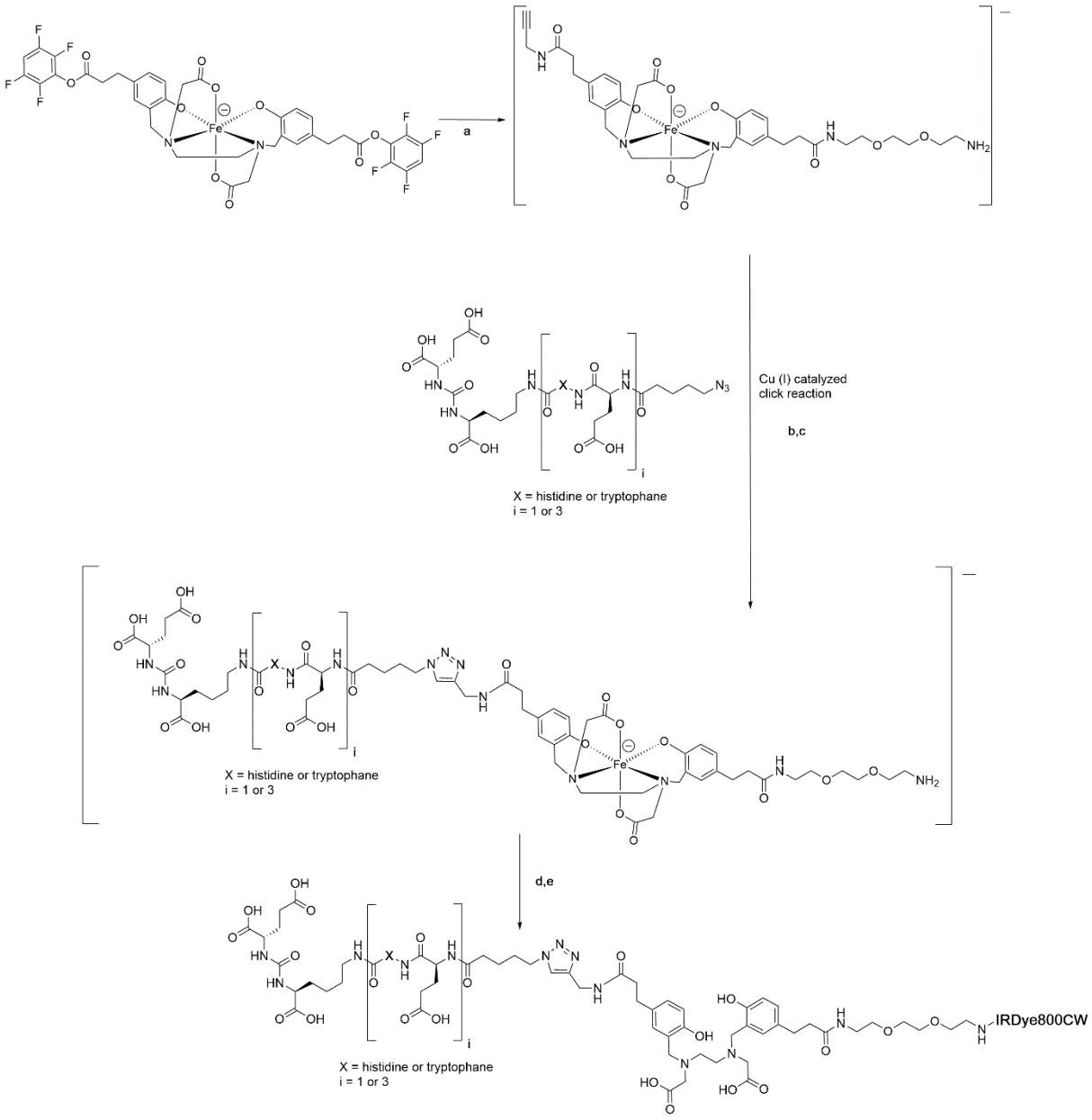

Supplemental Figure 1. Synthesis of Glu-urea-Lys-(HE)$_1$-HBED-CC-IRDye800CW, Glu-urea-Lys-(HE)$_3$-HBED-CC-IRDye800CW and Glu-urea-Lys-(WE)$_1$-HBED-CC-IRDye800CW. (a) 0.95 eq. 2-propynylamine, DIPEA, 4 h, RT; excess (100 µL) 2,2′-(ethylendioxy)bis(ethylamine), 16 h, RT, (b) 1 eq. CuSO4, (c) 1 eq. Na-ascorbate in THF/H_2O (1:1, v/v), RT, 16 h, (d) PBS-buffer (pH 8.5), 1 eq. IRDye800CW-NHS ester RT, 16 h, (e) 1 M HCl.

Synthesis of Glu-urea-Lys-HBED-CC-$(HE)_3$-IRDye800CW

In a first step PEG_2-$(EH)_3$-$CO(CH_2)_4$-N_3 was synthesized starting from an O-Bis(aminoethyl)ethylene glycol trityl resin. Based on a standard Fmoc solid phase protocol, Fmoc-L-Glu(O*t*-Bu)-OH and Fmoc-L-His(Trt)-OH (4 eq. each) were activated with HBTU (4 eq.) and DIPEA (4 eq.) and coupled in DMF. The couplings were repeated three times to obtain the $(HE)_3$-motif. Finally, 5-azidopentanoic acid (4 eq.) was coupled using HBTU (4 eq.) and DIPEA (4 eq.) in DMF. The azido-functionalized intermediate was cleaved from the resin for 3 hours at RT using TFA/TIPS/H_2O (95/2.5/2.5, v/v/v), the product purified with preparative HPLC and identified with mass spectrometry.

Subsequently, bis-TFP activated $[Fe(HBED\text{-}CC)]^-$ (**1**) was reacted with tris(*t*-Bu)-protected Glu-urea-Lys (ABX; 0.9 eq.) in DMF at RT (Supplemental Figure 2). After 4 h, 50 µL 2-propynylamine was added and the mixture stirred for 16 h at RT. The resulting Glu-urea-Lys([Fe(HBED-CC-propargylamin)]) was isolated via preparative HPLC (**2**). PEG_2-$(EH)_3$-$CO(CH_2)_4$-N_3 (1 eq.) and tris(*t*-Bu)-protected Glu-urea-Lys([Fe(HBED-CC-propargylamine)]) (1 eq.) were reacted via CuAAC, $CuSO_4$ (1 eq.), Na-ascorbate (1 eq.), in 3 mL THF/H_2O (1:1, v/v) for 16 h at RT. The tris(*t*-Bu)- and Fe-protected intermediate was separated by preparative HPLC and the tris(*t*-Bu)-protecting groups removed after lyophilisation with 3 mL TFA for 4 h at RT (**3**). In the final step IRDye800CW-NHS ester was conjugated to Glu-urea-Lys([Fe(HBED-CC-$(HE)_3$-PEG_2-NH_2)]) and complexed Fe^{3+} removed as described in the previous section (**4**).

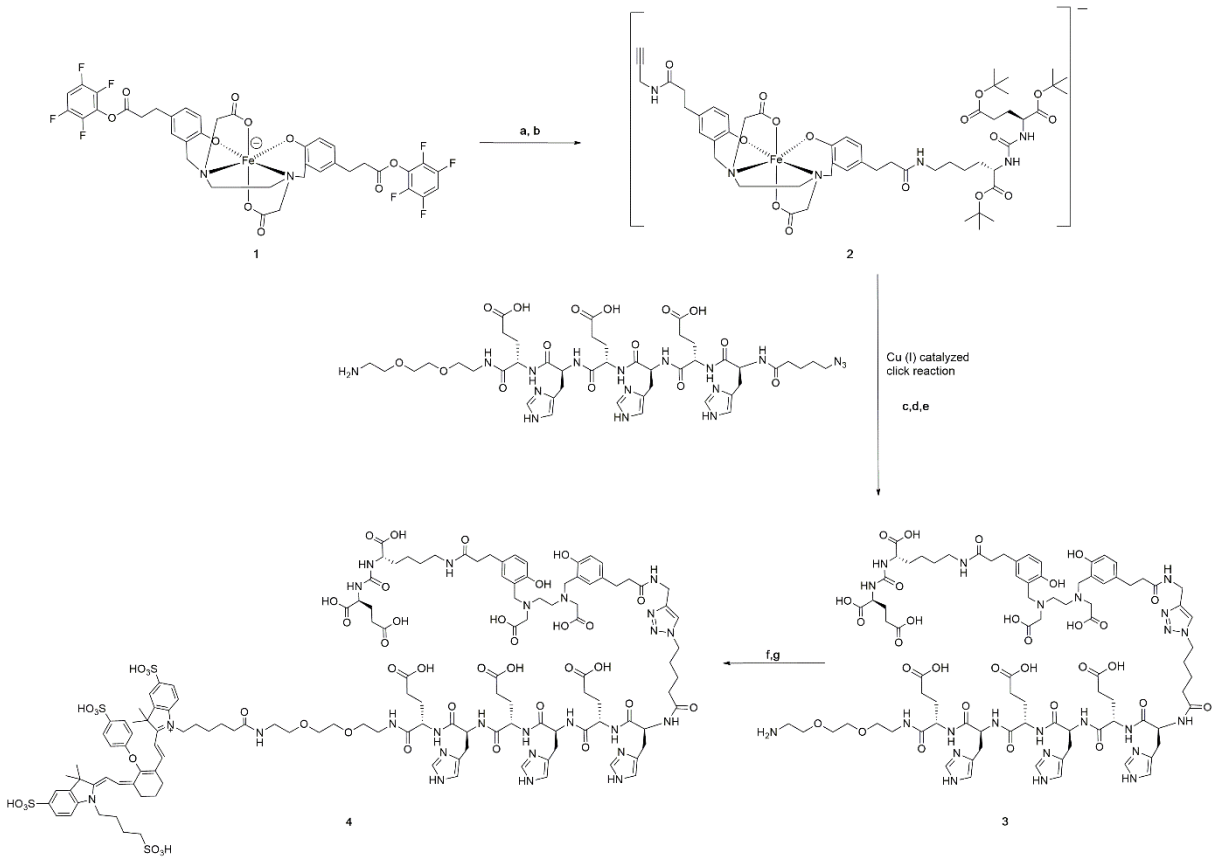

Supplemental Figure 2. Synthesis of Glu-urea-Lys-HBED-CC-(HE)$_3$-IRDye800CW. (a) 0.9 eq. tris(*t*-Bu)-protected Glu-urea-Lys in DMF, DIPEA, 4 h, RT (b) excess (50 µL) 2-propynylamine, 16 h, RT, (c) 1 eq. CuSO4, d) 1 eq. Na-ascorbate in THF/H_2O (1:1, v/v), RT, 16 h, (e) TFA, 3 h, RT, (f) PBS-buffer (pH 8.5), 1 eq. IRDye800CW-NHS ester RT, 16 h, (g) 1 M HCl.

Radiolabeling with ^{68}Ga and Determination of Lipophilicity

The precursor peptides [1 nmol in 2-[4-(2-hydroxyethyl)piperazin-1-yl]ethanesulfonic acid (HEPES) buffer (580 mg/ml) with 5 mg ascorbic acid, 90 µL] were added to 40 µL $^{68}Ga^{3+}$ eluate (~80-120 MBq). The pH was adjusted to 3.8 using 30% NaOH and 10% NaOH, respectively. The reaction mixture was incubated at 98°C for 10 minutes. The respective radiochemical yield was determined by reversed-phase high performance liquid chromatography (RP-HPLC) or reversed-phase thin layer chromatography (RP-TLC, 60 RP-18 F_{254S}) with 0.1 M sodium citrate [$HOC(COONa)(CH_2COONa)_2 \cdot 2H_2O$] as mobile phase. The 2-phase system n-octanol and PBS was used for the determination of lipophilicity of the ^{68}Ga-labeled compounds.

In Vitro Serum Stability

^{68}Ga-labeled Glu-urea-Lys-$(HE)_3$-HBED-CC-IRDye800CW (10 µL) was incubated in 100 µL human or mouse plasma (100 µL) at 37 °C. At different time points of incubation (t= 1 h, 2 h), aliquots of 10 µL were taken and plasma proteins precipitated in 30 µL acetonitrile. Samples were centrifuged for 5 min at 13000 rpm and the supernatants analysed by analytical RP-HPLC.

Preclinical Proof-of-Concept Study (PET and Optical Imaging)

The PET imaging study was performed with an Inveon µ-PET scanner (Siemens) with a dynamic scan for 60 min and a static scan (10 min) at 2 h p.i.. Transmission scans (10 min) were performed before the dynamic and static image acquisition, respectively. The images were reconstructed with the Inveon Acquisition Workspace Software (Siemens) and OSEM 3D SP-MAP algorithm (16 subsets, 4 iterations, MAP Iteration: 18) using a 28 frame protocol (2x15s,8x30s,5x60s,5x120s,8x300s) for the dynamic scan and one frame for the static scan. Median root was applied prior correction and images were converted to SUV images.

To identify the subcutaneous tumor by fluorescence, optical imaging was performed after PET imaging. Mice were sacrificed and the skin was removed covering the subcutaneous xenograft tumors. Subsequently, the Odyssey CLx system (LI-COR Biosciences, excitation wavelength 800 nm) was used for locating the tumor by fluorescence. Tumor tissue was resected and another scan performed with the Odyssey CLx system to ensure complete tumor tissue removal.

Supplementary Figures

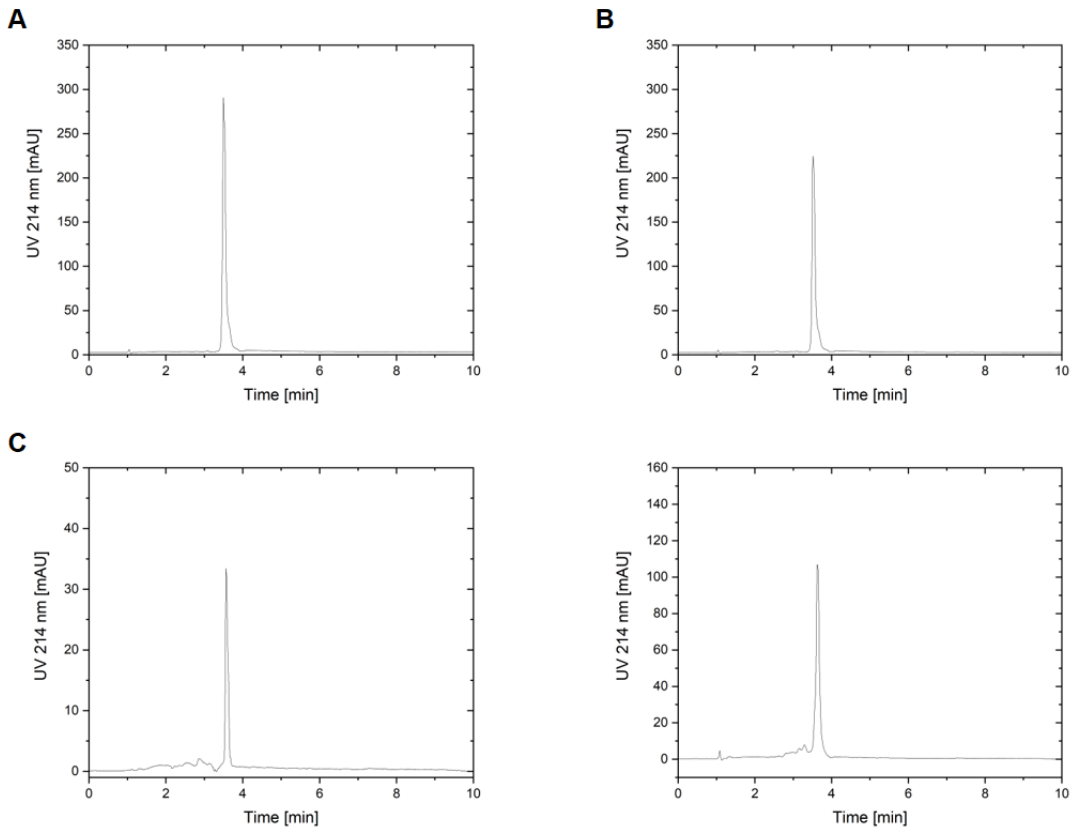

Supplemental Figure 3. Analytical HPLC of the compounds. Analytical reversed-phase HPLC of the final compounds was performed using a Chromolith RP-18e 100x4.6 mm column with a linear gradient (0.1% TFA in H_2O (A) to 100% B (0.1% TFA in CH_3CN)) in 10 min at 2 mL/min. UV trace at 214 nm is shown. (A) Glu-urea-Lys-$(HE)_1$-HBED-CC-IRDye800CW, (B) Glu-urea-Lys-$(WE)_1$-HBED-CC-IRDye800CW, (C) Glu-urea-Lys-$(HE)_3$-HBED-CC-IRDye800CW and (D) Glu-urea-Lys-HBED-CC-$(HE)_3$-IRDye800CW. Original data was plotted using OriginPro 2020 software.

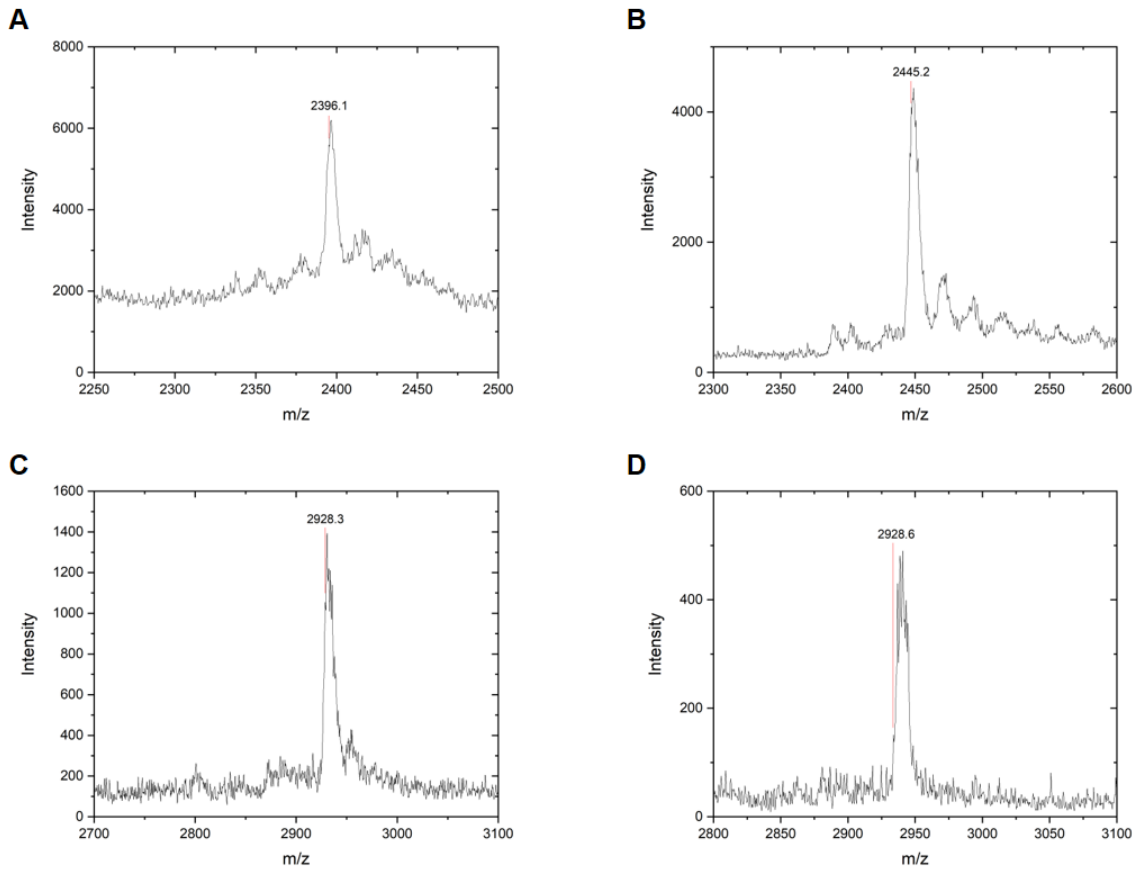

Supplemental Figure 4. MALDI spectra of the compounds. Mass spectrometry was performed with a MALDI-MS (Daltonics Microflex, Bruker Daltonics) and 2,5-dihydroxybenzoic acid as a matrix. (A) Glu-urea-Lys-$(HE)_1$-HBED-CC-IRDye800CW, (B) Glu-urea-Lys-$(WE)_1$-HBED-CC-IRDye800CW, (C) Glu-urea-Lys-$(HE)_3$-HBED-CC-IRDye800CW and (D) Glu-urea-Lys-HBED-CC-$(HE)_3$-IRDye800CW. Original data was plotted using OriginPro 2020 software.

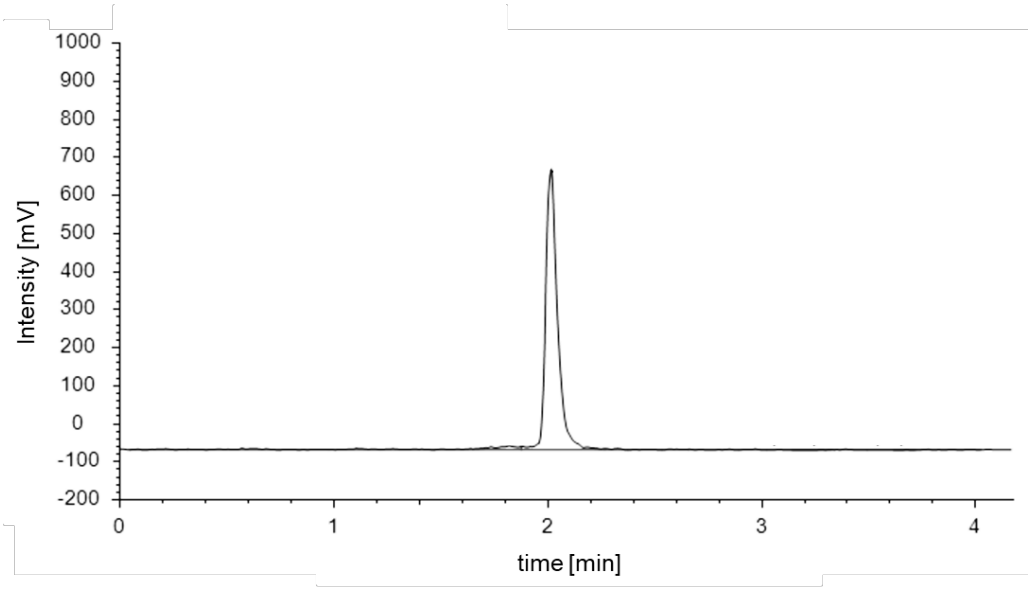

Supplemental Figure 5. Exemplary analytical radio-HPLC of ^{68}Ga-Glu-urea-Lys-(HE)$_3$-HBED-CC-IRDye800CW. Analytical reversed-phase HPLC of the ^{68}Ga-labeled compound was performed using a Chromolith RP-18e 100x4.6 mm column with a linear gradient (0.1% aqueous TFA (A) to 100% B (0.1% TFA in CH_3CN)) in 5 min at 4 mL/min. For radiodetection the system was equipped with a γ-detector.

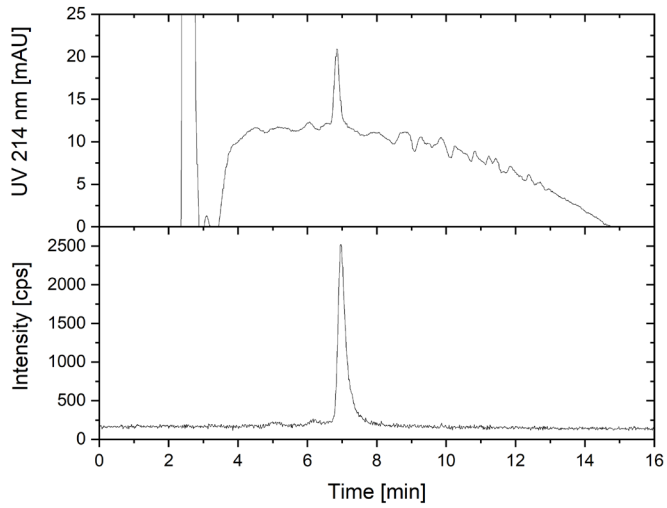

Supplemental Figure 6. HPLC of co-injected ^{68}Ga-Glu-urea-Lys-(HE)$_3$-HBED-CC-IRDye800CW and Glu-urea-Lys-(HE)$_3$-HBED-CC-IRDye800CW. Analytical reversed-phase HPLC of the ^{68}Ga-labeled compound co-injected with the non-radiolabeled precursor Glu-urea-Lys-(HE)$_3$-HBED-CC-IRDye800CW was performed using a EC 250/4.6 NUCLEOSIL 120-5 C 18 column (Machery-Nagel) with a linear gradient 85% 0.1% aqueous TFA (A) to 60% B (0.1% TFA in CH_3CN)) in 13 min at 1.5 mL/min. UV was measured at 214 nm and for radiodetection the system was equipped with a γ-detector. Original data was plotted using OriginPro 2020 software.

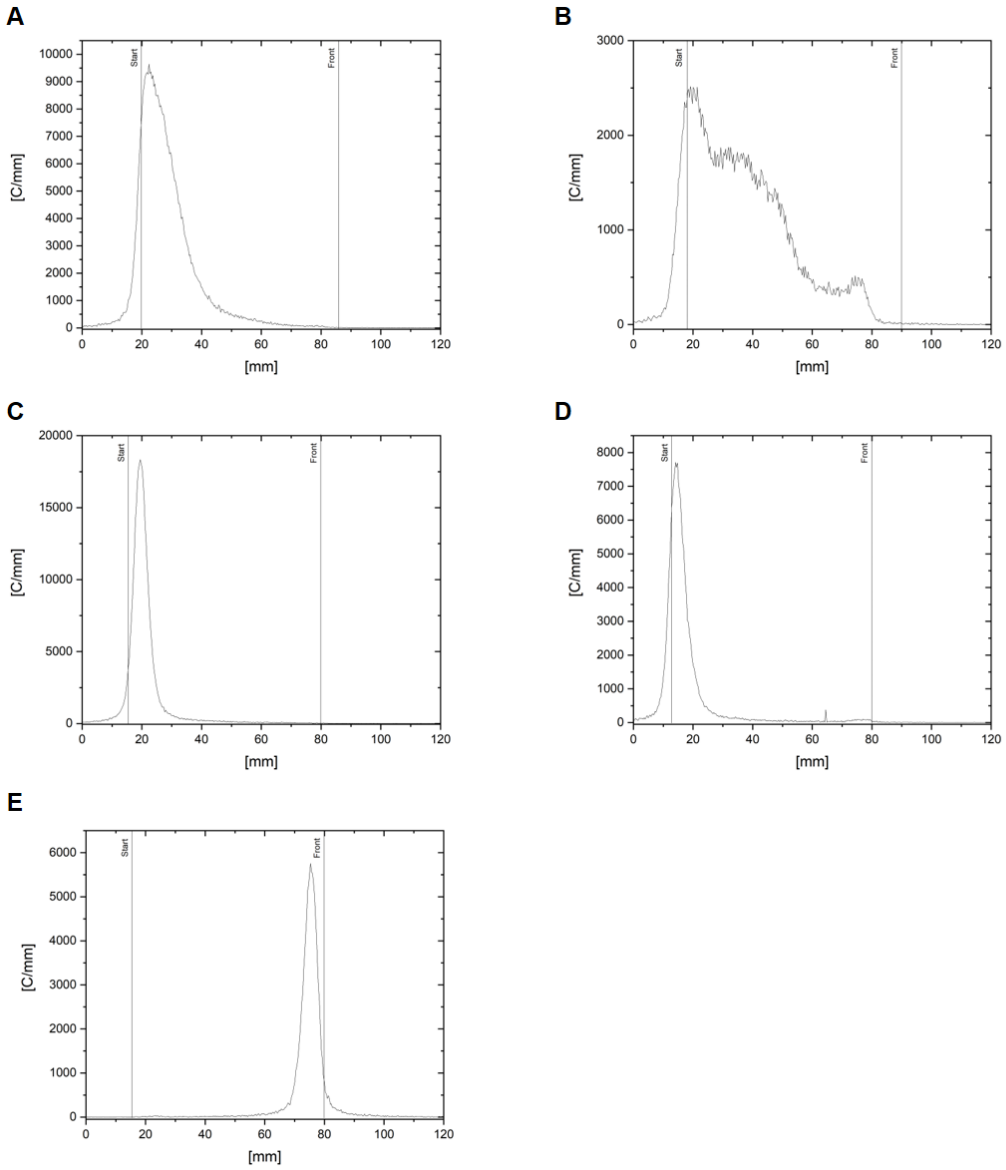

Supplemental Figure 7. Reversed-phase thin layer chromatography of ^{68}Ga-labeled compounds. RP-TLC (60 RP-18 F_{254S}) was performed with 0.1 M sodium citrate as mobile phase. (A) Glu-urea-Lys-$(HE)_1$-HBED-CC-IRDye800CW, (B) Glu-urea-Lys-$(WE)_1$-HBED-CC-IRDye800CW, (C) Glu-urea-Lys-$(HE)_3$-HBED-CC-IRDye800CW, (D) Glu-urea-Lys-HBED-CC-$(HE)_3$-IRDye800CW and (E) $^{68}GaCl_3$ as a control. Original data was plotted using OriginPro 2020 software.

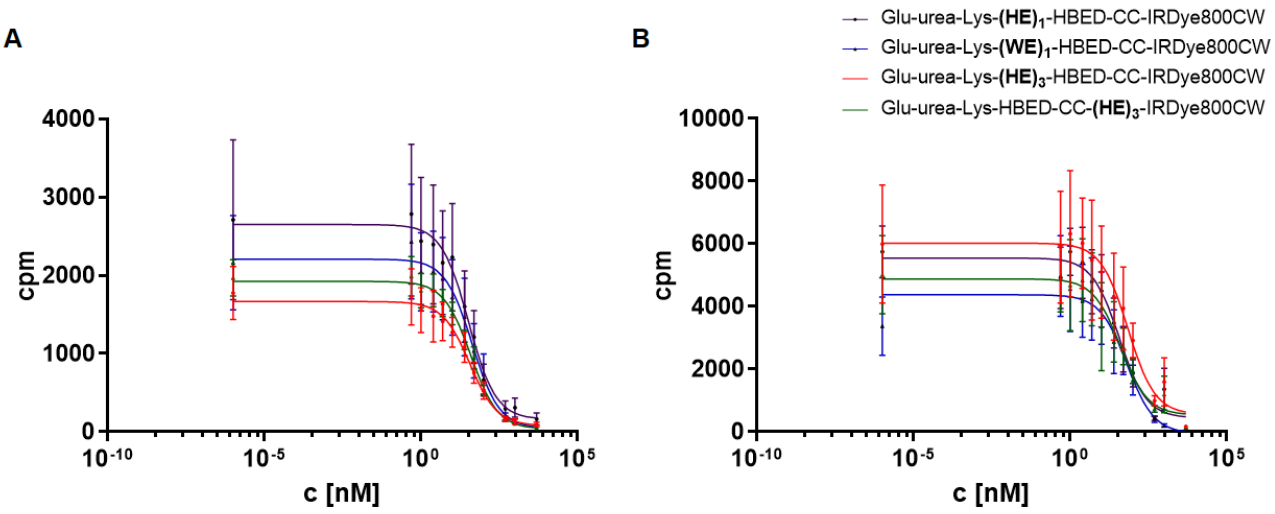

Supplemental Figure 8. Determination of binding affinity to PSMA. Binding affinity was determined on PSMA$^+$ LNCaP-cells with ^{68}Ga-PSMA-10 (K_d: 3.8 ± 1.8 nM (*1*), $c_{radioligand}$: 0.75 nM) as radioligand. IC_{50} curves of (A) free ligands and (B) $^{69/71}$Ga-labeled ligands were plotted with GraphPad Software. The 50% inhibitory concentration (IC50) values were calculated by fitting the data using a nonlinear regression algorithm (GraphPad Software).

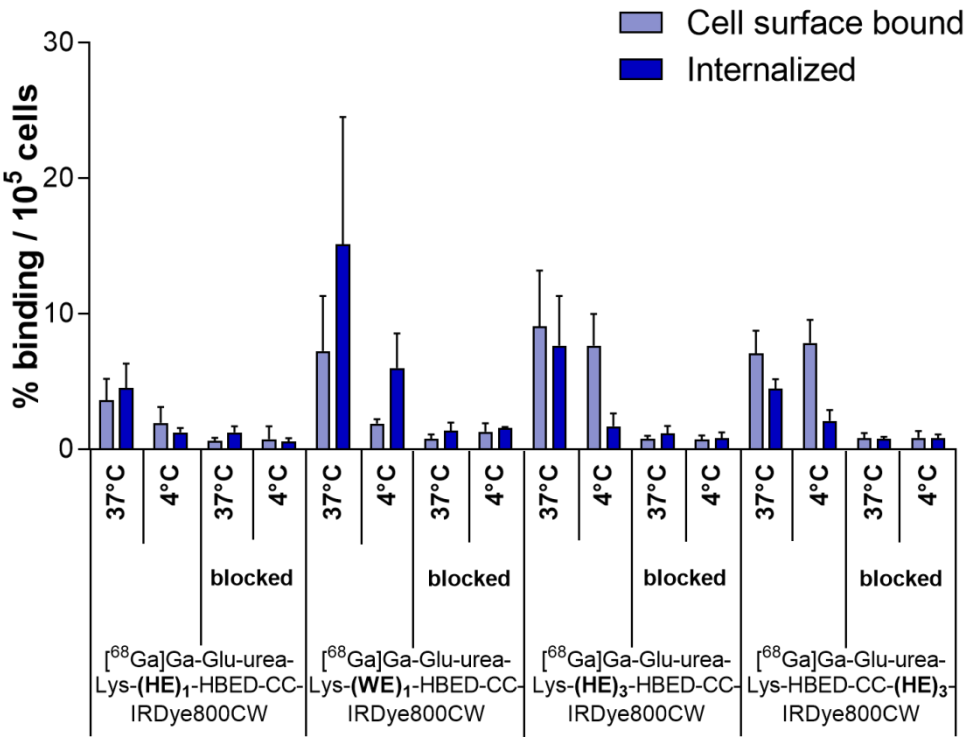

Supplemental Figure 9. Cell surface binding and internalization of ^{68}Ga-labeled compounds. Specificity of internalization was determined by blocking with 2-PMPA (500 µM) or incubating on ice at 4°C. Data are expressed in %binding/10^5 cells and represent mean ± standard deviation (n=3).

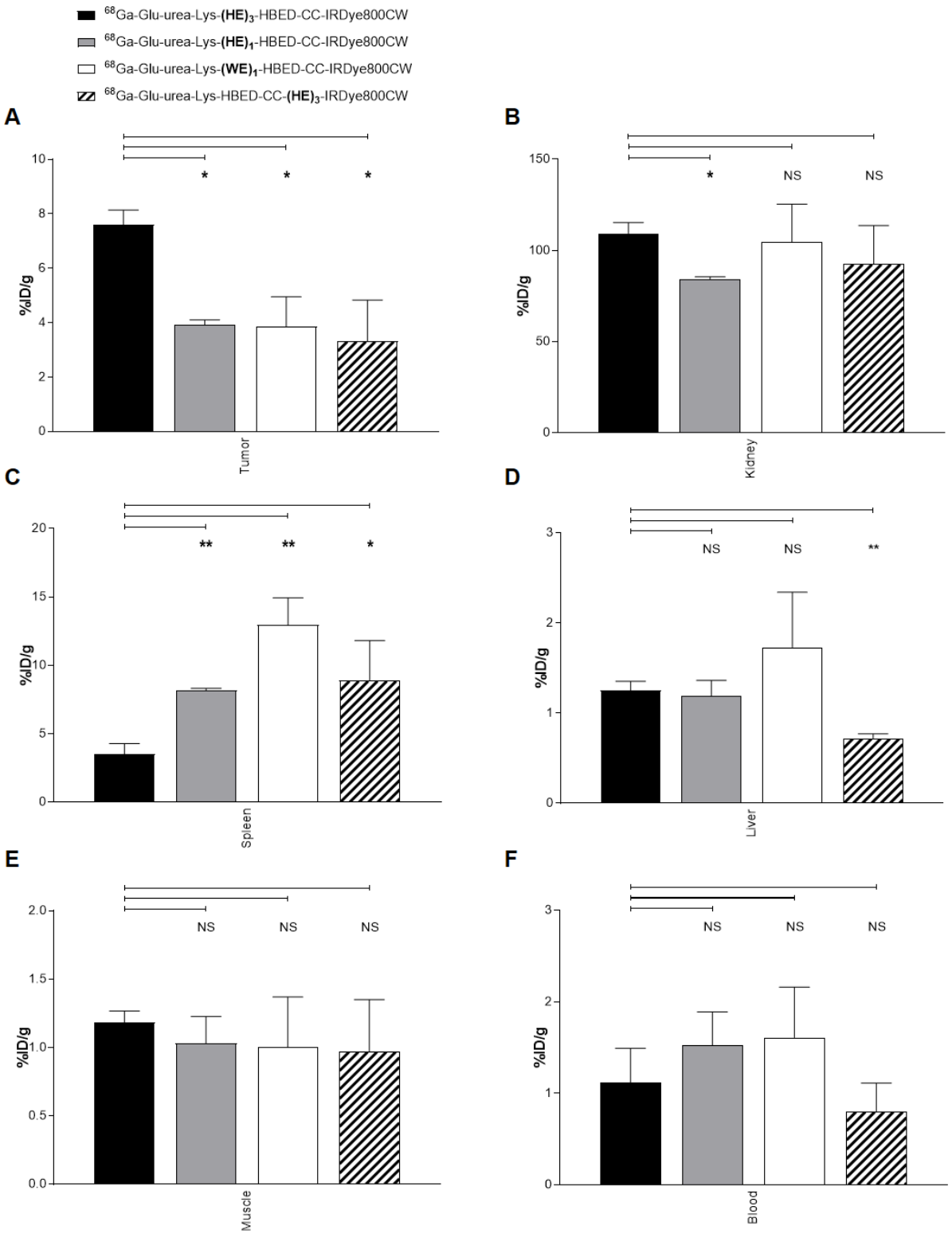

Supplemental Figure 10. Organ distribution of ^{68}Ga-labeled compounds. Organ distribution of 60 pmol ^{68}Ga-labeled compounds at 1 h p.i. with uptake in (A) PSMA^{+}-tumor (LNCaP), (B) kidney, (C) spleen, (D) liver, (E) muscle and (F) blood. Data are expressed as mean % ID/g tissue ± SD (n=3). Significant differences are presented with asterisks above the bars that are being compared (NS: not significant, *p<0.05, **p<0.01).

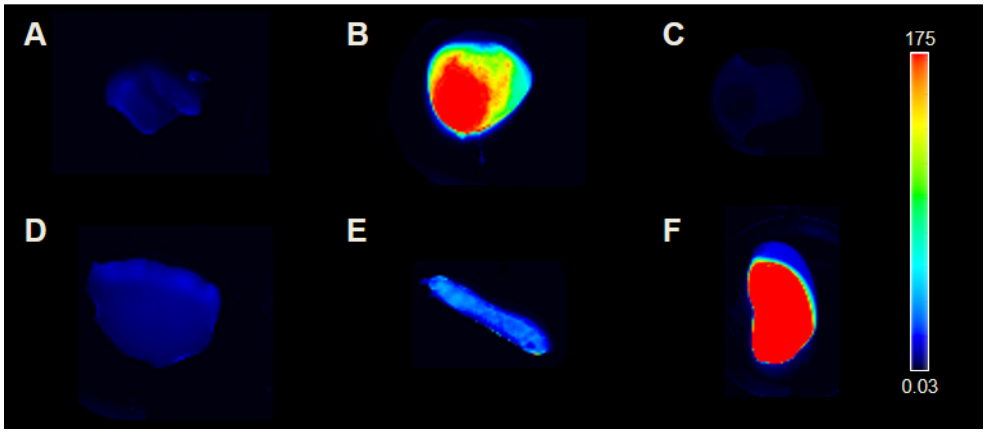

Supplemental Figure 11. Fluorescence imaging after organ distribution 1 h p.i.. Fluorescence imaging of organs dissected after injection of 0.5 nmol ^{68}Ga-labeled Glu-urea-Lys-(HE)$_3$-HBED-CC-IRDye800CW in LNCaP tumor-bearing BALB/c nu/nu mice 1 h p.i. (n=3, one representative image out of three is shown) acquired with the Odyssey CLx system (excitation wavelength 800 nm). Fluorescence intensity is presented in heat map colouring. (A) muscle, (B) PSMA$^+$-tumor (LNCaP), (C) blood (D) liver, (E) spleen, (F) kidney.

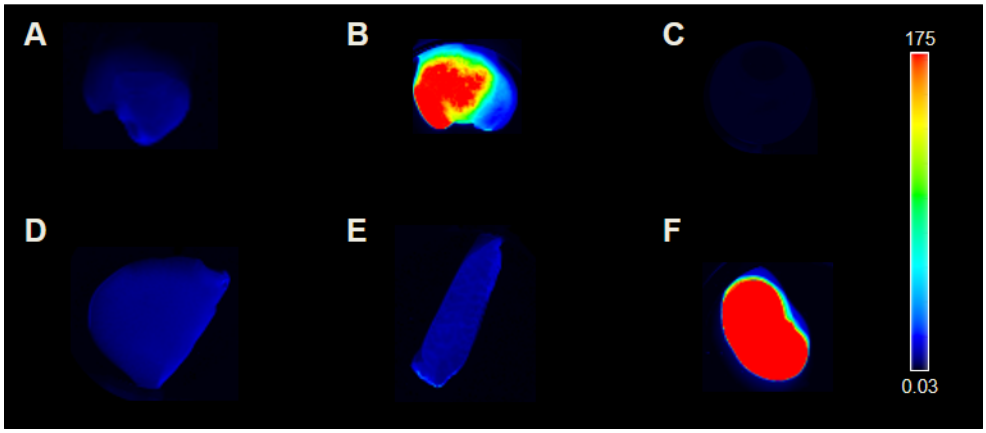

Supplemental Figure 12. Fluorescence imaging after organ distribution 2 h p.i.. Fluorescence imaging of organs dissected after injection of 0.5 nmol ^{68}Ga-labeled Glu-urea-Lys-(HE)$_3$-HBED-CC-IRDye800CW in LNCaP tumor-bearing BALB/c nu/nu mice 2 h p.i. (n=3, one representative image out of three is shown) acquired with the Odyssey CLx system (excitation wavelength 800 nm). Fluorescence intensity is presented in heat map colouring. (A) muscle, (B) PSMA$^+$-tumor (LNCaP), (C) blood (D) liver, (E) spleen, (F) kidney.

Supplementary Tables

Supplemental Table 1. Analytical data of the compounds.

Compound	Sum formula	m/z exact mass (calc.)	m/z*	Chemical yield [%]†	Lipophilicity log$D_{pH\ 7.4}$ *n-octanol/PBS*‡
Glu-urea-Lys-**(HE)$_1$**-HBED-CC-IRDye800CW	$C_{109}H_{144}N_{17}O_{36}S_4^+$	2394.9	2396.1	34	-3.15 ± 0.08
Glu-urea-Lys-**(WE)$_1$**-HBED-CC-IRDye800CW	$C_{114}H_{147}N_{16}O_{36}S_4^+$	2443.9	2445.2	12	-3.03 ± 0.05
Glu-urea-Lys-**(HE)$_3$**-HBED-CC-IRDye800CW	$C_{131}H_{172}N_{25}O_{44}S_4^+$	2927.1	2928.3	38	-1.65 ± 0.40
Glu-urea-Lys-HBED-CC-**(HE)$_3$**-IRDye800CW	$C_{131}H_{172}N_{25}O_{44}S_4^+$	2927.1	2928.6	17	-3.22 ± 0.08

* Mass spectrometry of non-labeled ligand detected as $[M+H]^+$, † Chemical yields refer to the fluorescent dye conjugation, ‡ Lipophilicity of ^{68}Ga-labeled ligand.

Supplemental Table 2. Chemical yields of the synthesis intermediates.

Intermediate	Chemical yield [%]
[Fe(HBED-CC-TFP$_2$)]	37
PEG$_2$-[Fe(HBED-CC-propargylamine)]	43
Glu-urea-Lys([Fe(HBED-CC-propargylamine)])	36
Glu-urea-Lys((HE)$_1$-CO(CH$_2$)$_4$-N$_3$)	66
Glu-urea-Lys((HE)$_3$-CO(CH$_2$)$_4$-N$_3$)	13
Glu-urea-Lys((WE)$_1$-CO(CH$_2$)$_4$-N$_3$)	58
PEG$_2$-(EH)$_3$-CO(CH$_2$)$_4$-N$_3$	35
Glu-urea-Lys((HE)$_1$-HBED-CC-PEG$_2$-NH$_2$)	15
Glu-urea-Lys((HE)$_3$-HBED-CC-PEG$_2$-NH$_2$)	23
Glu-urea-Lys((WE)$_1$-HBED-CC-PEG$_2$-NH$_2$)	16
Glu-urea-Lys([Fe(HBED-CC-(HE)$_3$-PEG$_2$-NH$_2$)])	13

Supplemental Table 3. Organ distribution of 0.06 nmol ^{68}Ga-labeled compounds in LNCaP-tumor bearing BALB/c nu/nu mice 1 h p.i.*.

	^{68}Ga-Glu-urea-Lys-**(HE)$_1$**-HBED-CC-IRDye800CW [%ID/g]	^{68}Ga-Glu-urea-Lys-**(WE)$_1$**-HBED-CC-IRDye800CW [%ID/g]	^{68}Ga-Glu-urea-Lys-**(HE)$_3$**-HBED-CC-IRDye800CW [%ID/g]	^{68}Ga-Glu-urea-Lys-HBED-CC-**(HE)$_3$**-IRDye800CW [%ID/g]
Blood	1.52 ± 0.64	1.61 ± 0.55	1.12 ± 0.64	0.80 ± 0.31
Heart	0.94 ± 0.14	1.49 ± 0.51	1.36 ± 0.37	0.57 ± 0.26
Lung	2.46 ± 0.46	2.57 ± 1.01	2.34 ± 0.37	1.78 ± 1.19
Spleen	8.17 ± 0.23	12.94 ± 2.00	3.47 ± 1.39	8.88 ± 2.93
Liver	1.19 ± 0.30	1.73 ± 0.61	1.25 ± 0.18	0.72 ± 0.05
Kidney	84.34 ± 2.13	104.58 ± 20.79	109.27 ± 10.33	92.54 ± 21.07
Muscle	1.03 ± 0.34	1.00 ± 0.37	1.18 ± 0.15	0.97 ± 0.38
Intestine	1.29 ± 0.36	0.96 ± 0.37	1.31 ± 0.00	0.65 ± 0.21
Brain	0.30 ± 0.10	0.15 ± 0.04	0.18 ± 0.02	0.18 ± 0.06
Tumor	3.92 ± 0.31	3.85 ± 1.10	7.59 ± 0.95	3.32 ± 1.51

***** Data are expressed as mean % ID/g tissue ± SD (n=3).

Supplemental Table 4. Tumor-to-organ ratios of 0.06 nmol ^{68}Ga-labeled compounds in LNCaP-tumor bearing BALB/c nu/nu mice 1 h p.i.*.

	^{68}Ga-Glu-urea-Lys-**(HE)$_1$**-HBED-CC-IRDye800CW	^{68}Ga-Glu-urea-Lys-**(WE)$_1$**-HBED-CC-IRDye800CW	^{68}Ga-Glu-urea-Lys-**(HE)$_3$**-HBED-CC-IRDye800CW	^{68}Ga-Glu-urea-Lys-HBED-CC-**(HE)$_3$**-IRDye800CW
Blood	3.01 ± 1.00	2.42 ± 0.21	8.81 ± 4.67	4.23 ± 1.02
Heart	4.39 ± 0.34	2.63 ± 0.34	5.72 ± 0.64	6.15 ± 1.56
Lung	1.69 ± 0.37	1.55 ± 0.23	3.27 ± 0.39	2.09 ± 0.46
Spleen	0.49 ± 0.03	0.30 ± 0.07	2.34 ± 0.47	0.38 ± 0.10
Liver	3.51 ± 0.86	2.26 ± 0.18	6.09 ± 0.13	4.61 ± 1.72
Kidney	0.05 ± 0.00	0.04 ± 0.01	0.07 ± 0.00	0.03 ± 0.01
Muscle	4.14 ± 1.32	3.96 ± 0.70	6.45 ± 0.09	3.51 ± 0.77
Intestine	3.35 ± 1.03	4.12 ± 0.38	5.80 ± 0.60	5.14 ± 1.15
Brain	14.97 ± 5.85	25.43 ± 2.13	42.66 ± 1.98	17.62 ± 2.14

***** Data are expressed as mean tumor-to-organ ratio ± SD (n=3).

Supplemental Table 5. Organ distribution of 0.06 nmol ^{68}Ga-labeled Glu-urea-Lys-(HE)$_3$-HBED-CC-IRDye800CW in PC-3-tumor bearing BALB/c nu/nu mice 1 h p.i.*.

	^{68}Ga-Glu-urea-Lys-**(HE)$_3$**-HBED-CC-IRDye800CW [%ID/g]	^{68}Ga-Glu-urea-Lys-**(HE)$_3$**-HBED-CC-IRDye800CW Tumor-to-Organ ratio
Blood	0.90 ± 0.21	0.58 ± 0.10
Heart	0.60 ± 0.21	0.88 ± 0.09
Lung	0.90 ± 0.36	0.60 ± 0.05
Spleen	1.30 ± 0.70	0.45 ± 0.08
Liver	0.53 ± 0.18	1.01 ± 0.04
Kidney	60.14 ± 32.59	0.01 ± 0.003
Muscle	0.21 ± 0.06	2.51 ± 0.20
Intestine	0.50 ± 0.23	1.11 ± 0.15
Brain	0.04 ± 0.01	14.33 ± 1.88
Tumor	0.53 ± 0.18	-

***** Data are expressed as mean % ID/g tissue ± SD (n=3) and Tumor-to-Organ ratios.

Supplemental Table 6. Organ distribution of 0.06 nmol ^{68}Ga-labeled Glu-urea-Lys-(HE)$_3$-HBED-CC-IRDye800CW in LNCaP-tumor bearing BALB/c nu/nu mice 2 h p.i.*.

	^{68}Ga-Glu-urea-Lys-**(HE)$_3$**-HBED-CC-IRDye800CW [%ID/g]	^{68}Ga-Glu-urea-Lys-**(HE)$_3$**-HBED-CC-IRDye800CW Tumor-to-Organ ratio
Blood	0.65 ± 0.01	4.73 ± 1.42
Heart	0.53 ± 0.08	5.84 ± 1.45
Lung	0.89 ± 0.05	3.43 ± 0.89
Spleen	0.76 ± 0.16	4.02 ± 0.70
Liver	0.76 ± 0.11	4.01 ± 0.77
Kidney	55.81 ± 9.76	0.06 ± 0.01
Muscle	0.47 ± 0.11	6.50 ± 0.95
Intestine	0.67 ± 0.17	4.66 ± 1.05
Brain	0.23 ± 0.15	14.83 ± 3.24
Tumor	3.10 ± 1.17	-

***** Data are expressed as mean % ID/g tissue ± SD (n=3) and Tumor-to-Organ ratios.

Supplemental Table 7. Organ distribution of 0.5 nmol ^{68}Ga-labeled Glu-urea-Lys-(HE)$_3$-HBED-CC-IRDye800CW in LNCaP-tumor bearing BALB/c nu/nu mice 1 h p.i.*.

	^{68}Ga-Glu-urea-Lys-**(HE)$_3$**-HBED-CC-IRDye800CW [%ID/g]	^{68}Ga-Glu-urea-Lys-**(HE)$_3$**-HBED-CC-IRDye800CW Tumor-to-Organ ratio
Blood	3.10 ± 1.40	6.89 ± 0.62
Heart	2.64 ± 0.59	7.87 ± 0.60
Lung	4.27 ± 1.02	4.96 ± 0.95
Spleen	6.90 ± 3.21	3.15 ± 0.62
Liver	2.43 ± 0.62	8.55 ± 0.61
Kidney	229.08 ± 53.38	0.09 ± 0.01
Muscle	1.17 ± 0.13	17.84 ± 2.26
Intestine	2.66 ± 0.89	7.89 ± 0.32
Brain	0.15 ± 0.06	144.46 ± 27.52
Tumor	20.98 ± 6.54	-

***** Data are expressed as mean % ID/g tissue ± SD (n=3) and Tumor-to-Organ ratios.

Supplemental Table 8. Organ distribution of 0.5 nmol ^{68}Ga-labeled Glu-urea-Lys-(HE)$_3$-HBED-CC-IRDye800CW in LNCaP-tumor bearing BALB/c nu/nu mice 2 h p.i.*.

	^{68}Ga-Glu-urea-Lys-**(HE)$_3$**-HBED-CC-IRDye800CW [%ID/g]	^{68}Ga-Glu-urea-Lys-**(HE)$_3$**-HBED-CC-IRDye800CW Tumor-to-Organ ratio
Blood	1.91 ± 0.84	6.56 ± 0.98
Heart	1.34 ± 0.73	9.45 ± 0.72
Lung	2.07 ± 0.89	6.04 ± 0.94
Spleen	2.26 ± 1.16	5.57 ± 0.50
Liver	1.62 ± 0.86	7.79 ± 0.75
Kidney	176.10 ± 97.86	0.07 ± 0.01
Muscle	0.56 ± 0.37	23.08 ± 0.81
Intestine	1.30 ± 0.56	9.91 ± 2.18
Brain	0.09 ± 0.05	138.96 ± 25.36
Tumor	12.90 ± 8.46	-

***** Data are expressed as mean % ID/g tissue ± SD (n=3) and Tumor-to-Organ ratios.

References

1. Schafer M, Bauder-Wust U, Leotta K, et al. A dimerized urea-based inhibitor of the prostate-specific membrane antigen for 68Ga-PET imaging of prostate cancer. *EJNMMI Res.* 2012;2:23.

2. Eder M, Wangler B, Knackmuss S, et al. Tetrafluorophenolate of HBED-CC: a versatile conjugation agent for 68Ga-labeled small recombinant antibodies. *Eur J Nucl Med Mol Imaging.* 2008;35:1878-1886.